Response to the referees

Dear editor and referees,

We sincerely appreciate the time and attention you have devoted to our manuscript. Your comments and suggestions were very helpful in improving our manuscript. We have responded to all the referees' comments regarding our manuscript titled "Source apportionment of atmospheric water over East Asia – a source tracer study in CAM5.1". Please find our responses below:

Referee #1:

Summary:

This paper describes the implementation of a new Atmospheric Water Tracer (AWT) scheme in the NCAR Community Atmosphere Model Version 5.1 (CAM5.1). This new feature is then used to examine the sources of precipitation and water vapor for the Yangtze River Valley, Southern China, and the South China Sea. It is found that the North Atlantic, Northwest Pacific, and Northern Indian Ocean are the dominant moisture sources for the three regions, along with evaporation from Asia itself. In particular, it is found that the Indian ocean-based moisture sources tended to be largest in summer, during the monsoons, while the Pacific was the largest source during the rest of the year.

Recommendation:

The application of atmospheric water tracers to the Southeast Asian region is certainly interesting, and can provide new insights into the hydrological cycle and processes of this important region. However, there is potentially one major flaw in the implementation of the water tracers in CAM5.1 that must be addressed before it is fully accepted, as well as a few other concerns that are listed in the next few sections. Thus I am recommending major revisions for this article. Once these issues have been dealt with, then I believe the paper will be ready for publication.

Major issues:

1. This is not an issue in terms of the science presented here, but it is important to note that water tracers already exist in CAM5, up through CAM5.3, and is at least partially described here: http://onlinelibrary.wiley.com/doi/10.1002/2016MS000649/full

Thus although this does not take away from the science results presented here, it might be more beneficial if this work was presented in a less model-development focused journal, as these particular developments have already been done for this same model.

Reply: The atmospheric water tracers (AWTs) method implemented in CAM5.1 in our manuscript is entirely developed by ourselves. The AWTs method in our manuscript enables the CAM5 model to quantitatively trace the behaviour of atmospheric water substances originating from their moisture source region. We believe that our method is a technical improvement to the CAM5.1 model and is of interest to the readership of the GMD journal.

The method used in Singh et al. (2016) provides a similar feature regarding the atmospheric water tagging problem, although there may be some differences in the treatments of the relevant water tagging calculations (the details of the water tracer method are partially described in their paper). We believe that the two methods improve the CAM5 model system. We are also very pleased to communicate with Singh and other researchers through which we can further improve the water tracer method.

2. If am understanding your description of the water tracer implementation correctly, then the way you are treating the water tag tendencies from deep convection is sadly not valid, and will cause mass conservation issues which could put into question the scientific results shown here. The reason is because the convective tendency is partly generated by the transport of water vapor in the vertical, which may not have the same water tracer ratio as the level at which you are calculating the tendency. Thus this change in the ratio will result in the implicit addition or removal of water mass. For example, one component of the deep convective vapor tendency is:

$$\frac{\partial q_v}{\partial t} = \frac{\partial}{\partial z}(M_u q_u)$$

Using your formulation, the resulting tag equation would be:

$$\frac{\partial q_{v,tg}^k}{\partial t} = R\frac{\partial q_v}{\partial t} = R\left(\frac{\partial}{\partial z}(M_u q_u)\right), \qquad R = \frac{q_{v,tg}^k}{\sum_{k=1}^n q_{v,tg}^k}$$

Discretizing the vertical derivative results in something akin to:

$$\frac{\partial q_{v,tg}^k}{\partial t} = R\left(\frac{(M_{z_2}q_{z_2} - M_{z_1}q_{z_1})}{z_2 - z_1}\right) = \frac{(M_{z_2}Rq_{z_2} - M_{z_1}Rq_{z_1})}{z_2 - z_1}$$

Which shows that the only way your formulation can work is if the water tag ratios were exactly the same for both vertical levels on which the deep convection is being applied, which is almost certainly not true. Otherwise, the

assumed ratio will be different than the actual water tag ratio, and thus result in a mass conservation error. The only way to eliminate this problem is to have the water tracer tendency calculated in the exact same way as regular water, e.g.:

$$\frac{\partial q_{v,tg}^k}{\partial t} = E_{tg}^k - C_{tg}^k - \frac{1}{\rho}\frac{\partial}{\partial z}\left(M_u q_{u,tg}^k + M_d q_{d,tg}^k - M_c q_{v,tg}^k\right)$$

where the phase changes are calculated using the ratio method you described:

$$C_{tg}^k = \left(\frac{q_{v,tg}^k}{\sum_{k=1}^n q_{v,tg}^k}\right)C$$

If this is how you are actually doing it, then I would recommend just re-wording this section. However, if this is an issue, then I must recommend you either modify your existing algorithms to fix this issue, or simply re-do your experiments with the already existing water tracer implementation present in CAM5. Finally, I should note that the reason this error may not be showing up in your supplemental error figures is because you are examining the sum of all your water tags, and not the individual tags themselves (and thus allowing mass conservation errors of different signs to cancel each other out).

Reply: Thank you for your suggestion. This is an important improvement to our study. In the revised manuscript, we have modified the algorithms to fix this issue following your suggestion. Further, we performed our experiments again and we have added new results in the revised manuscript. Though there are some changes in numerical results, the qualitative conclusions remain unchanged.

Changes in manuscript: Please see Sect. 2.1 in the revised manuscript, which describe the tagged water vapour tendency in the deep convection scheme. Please also see the new numerical results in abstract and Sects. 3.3–4 in the revised manuscript.

Minor issues:

1. On line 27, I would avoid stating that water vapour is the most important component of the atmosphere, as that is probably just one's opinion. Instead maybe say something like "water vapour is one of the most important components of the atmosphere".

Reply: Thank you for your suggestion. We have revised this sentence following your suggestion in the revised manuscript.

2. It is unclear to me how you are calculating the water tracer vapor tendency produced by the shallow convection, as most of the description focuses solely on the condensate. Could you add a sentence or two describing the shallow convection's water tracer vapor tendency? Also, if it is implemented in the same way as the deep convection, then the major issue described above will also need to be dealt with for the shallow convection as well.

Reply: Thank you for your suggestion. The implementation of the shallow convection's water tracer vapour tendency is different from that of the deep convection. The mass mixing ratio (MMR) of the total water is assumed to be a conserved quantity in non-precipitating moist adiabatic processes within the shallow convection scheme. This assumption is also applied to the MMR of the tagged total water. Therefore, the tendency of tagged water vapour is computed as the difference between the tendency of tagged total water and the tendencies of tagged condensates in non-precipitating processes within the shallow convection scheme, similar to the calculation of the tendency of water vapour.

Changes in manuscript: We have added similar sentences to describe the shallow convection's tagged water vapour tendency in Sect. 2.2 in the revised manuscript.

3. In Section 2.7, it is stated that the sum of all tagged water tendencies should be equal to the tendency of the standard water model substance. However, it is unclear what occurs if this rule is violated. In particular, if this requirement is not met, what is done to the individual water tracers themselves in order to ensure that the summed tendencies are brought back to the value of the standard water tendency?

Reply: (a) If the summed tendencies of the tagged water substances are not equal to the tendencies of the corresponding original water substances in one physical parameterization, calculations of the tendencies of tagged water substances in other parameterizations may be affected as there are interactions among various physical and dynamical processes in CAM5.1. Clear differences between the summed MMRs of tagged water substances and the MMRs of original water substances may occur as shown in Fig. S6. We have added several sentences in Sect. 2.7 in the revised manuscript to state what may occur if the rule is violated.

(b) We have rewritten the description of the adjustment criteria, ensuring that the summed tendencies are returned to the value of the standard water tendency. Equations (42) and (43) have also been added to express these adjustments. Please see Sect. 2.7 in the revised manuscript, in which we have implemented these changes.

4. One line 537, I would replace "(colours, unit: 1)" with "(colours, unit: ratio of tagged precip over total precip)", or at least something that is more descriptive than just the number one. I would do the same for the "unit: 1" reference in Figure 5 as well.

Reply: Thank you for your suggestion. We have replaced "(colours, unit: 1)" with "(colours, unit: ratio of tagged precipitation over total precipitation)" in the captions of Figure 3 and Figure 5 in the revised manuscript.

5. I would describe what the vectors are in the caption of Figure 3 as is done in the main text.

Reply: Thank you for your suggestion. The vectors have been described in the caption of Figure 3 in the revised manuscript.

6. In Figure 5b, it is difficult to tell which pink contour corresponds to the "0.2" amount, as the label overlaps multiple contour lines. If possible, can you shift the label over such that it is more clear which contour line it is referring to? Possibly making the label smaller might also help in this situation as well.

Reply: Thank you for your suggestion. We have decreased the size of the label and increased the density of the label for the pink contour in Figure 5 in the revised manuscript.

7. It might be good to include some sort of legend for Figures 6, 7, and 8 that re-states which water tag each color corresponds to. This will help lessen the reader's need to constantly go back to Figure 1 to determine what water tag each color represents.

Reply: Thank you for your suggestion. We have added legends for Figures 6, 7, and 8 in the revised manuscript.

Grammatical issues:

1. Need to make sure that when you have list of three or more objects in a sentence, that commas are used like so: x, y, and z Instead, you often times have: x, y and z This makes it seem that y and z are together as one idea, when in reality they are separate. So, just make sure to have a comma before the "and" whenever a list is involved.

Reply: Thank you for your suggestion. We have checked our manuscript carefully and modified the sentences with the aforementioned problem in the revised manuscript.

2. On lines 81 and 82, replace "isotope data not only reflect the water cycle" with "isotope data reflects more than just the water cycle". The reason being that "not only" is a conjunction I believe, and so the phrase would need a ",but" at the end, as in "not only x, but also y".

Reply: Thank you for your suggestion. We have replaced "isotope data not only reflect the water cycle" with "isotope data reflects more than just the water cycle" in Sect. 1 in the revised manuscript.

3. On line 82, I would replace "and that sensitivity" with just "and sensitivity".

Reply: Thank you for your suggestion. We have replaced "and that sensitivity" with just "and sensitivity" in the revised manuscript.

4. On lines 97 and 99, replace "Neal" with "Neale".

Reply: Thank you for your suggestion. We have replaced "Neal" with "Neale" in the revised manuscript.

5. On line 222, I would replace "sum MMRs" with "summed MMRs".

Reply: Thank you for your suggestion. We have replaced "sum MMRs" with "summed MMRs" in Sect. 2.7 in the revised manuscript.

6. On line 241, I would replace "compared with" with "compared to".

Reply: Thank you for your suggestion. We have replaced "compared with" with "compared to" in Sect. 3.1 in the revised manuscript.

7. On line 266, I would replace "over the North Africa" with just "over North Africa".

Reply: Thank you for your suggestion. We have replaced "over the North Africa" with "over North Africa" in the second paragraph of Sect. 3.2 in the revised manuscript.

8. On line 366, I would replace "NAO" with "North Atlantic Ocean", as none of the other regional acronyms are used in this particular sentence.

Reply: Thank you for your suggestion. We have replaced "NAO" with "North Atlantic Ocean" in the first paragraph of Sect. 4 in the revised manuscript.

9. On line 390, I would replace "over few regions" with "over a few regions". It might also be beneficial to spell out NAM instead of using the acronym here, although that is probably just personal preference.

Reply: Thank you for your suggestion. We have replaced "over few regions" with "over a few regions". "NAM" has also been replaced by "North America". Please check them in the last paragraph of Sect. 4 in the revised manuscript.

Referee 2#:

This study uses CAM5.1 to identify the sources of moisture contributing to the precipitation in East Asia. Both approach and results are interesting. The manuscript may be accepted for publication in GMD after major revision. Specific comments are listed below.

Major comments:

I. Diagnostics part:

1. It is clear how the simulation were conducted. The simulation were conducted from 1997-2007. It is said in line 284 that "…CAM5.1 is driven by MERRA data …". Obviously, it was not an AMIP-type experiment. Please provide clear discussion the simulation procedure and how the MERRA data were applied to drive CAM5.1. Also what does "offline version of CAM5.1" mean?

Reply: Thank you for your suggestion.

(a) The basic simulation setup is identical to that in Lamarque et al. (2012). We have cited the work of Lamarque et al. (2012) instead of restating it again. Please see the second paragraph in Sect. 2 in the revised manuscript: "The basic simulations setup, including emissions and upper and lower boundary conditions, is identical to that of the specified dynamics simulations of CAM5 in Lamarque et al. (2012). In this study, the wet removal scheme in Horowitz et al. (2003) is adopted."

(b) The zonal and meridional wind components, air temperature, surface pressure, surface temperature, surface geopotential, surface stress, and sensible and latent heat fluxes are read from the MERRA datasets to drive CAM5.1. All input fields are linearly interpolated at timesteps between the reading times to prevent jumps. Subsequently, these fields are used to drive the CAM5.1's parameterizations to generate the necessary variables and calculate subgrid scale transport and the hydrological cycle (Lamarque et al., 2012). We have provided these descriptions of how the MERRA data were applied to drive CAM5.1. Please check it in Sect. 2.5 in the revised manuscript.

(c) "Offline version of CAM5.1" means that the CAM5.1 model is driven by external meteorological fields. In the revised manuscript, we have replaced "precipitation simulated by the offline version of CAM5.1" with "precipitation in the specified dynamics simulation of CAM5.1" in Sect. 3.1 in the revised manuscript.

2. In addition to comparing the simulated precipitation with GPCC, a comparison of simulated water substances and convective/stratiform precipitation with satellite observation could be useful and informative. Also, assessments on other parts of water cycle, such as the evaporation, surface water storage, and their seasonal cycles (e.g. Numaguti

1999) should also be checked. The bias of model simulated large-scale circulation and their possible impacts on the results should also be discussed.

Reply: Thank you for your suggestion.

(a) In the revised manuscript, we have added the comparison between the Atmospheric Infrared Sounder (AIRS) observed and CAM5.1 simulated water vapour for the years from 2003 to 2007. In general, the simulated water vapour is well consistent with measured values. Please see Sect. 3.1 in the revised manuscript and Fig. S7 in the supplementary information. In addition, the corresponding conclusion has also been added in Sect. 4 in the revised manuscript.

(b) We compared the cloud water content from AIRS and CAM5.1 simulation results. Please see Fig. R1 below. Overall the cloud water pattern and amount over oceans around Eurasia can be characterized by CAM5.1, but there are some shifts for the high cloud water centres (e.g. over Northwest Pacific) in the model.
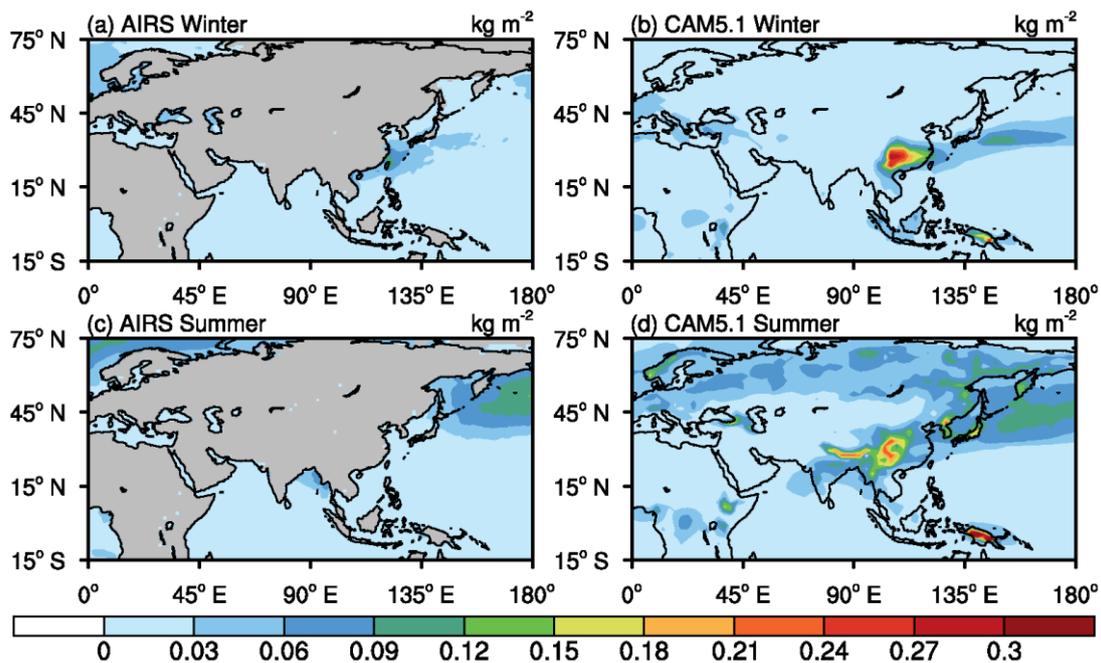
Figure R1. Comparison between (left) AIRS observed and (right) CAM5.1 simulated cloud water content (unit: kg m^{-2}) during (top) winter and (bottom) summer. All results are 5-year averages for 2003–2007. Grey areas indicate where required data are not available.

(c) Figure R2 shows the comparison between the Microwave Limber Sounder (MLS) observed and simulated cloud ice content at 215 hPa. There is significant lower bias in the simulated result. Waliser et al. (2009) pointed out that the accurate simulation of cloud ice in global circulation models (GCMs) is still a challenge to model development. Because the poor representation of cloud ice in the model, the source apportionment of cloud ice in CAM5.1 cannot

provide valid results. However, the total precipitation and water vapour can be reproduced well by CAM5.1; therefore results and discussions in this manuscript focused on the source apportionments of total precipitation and water vapour.
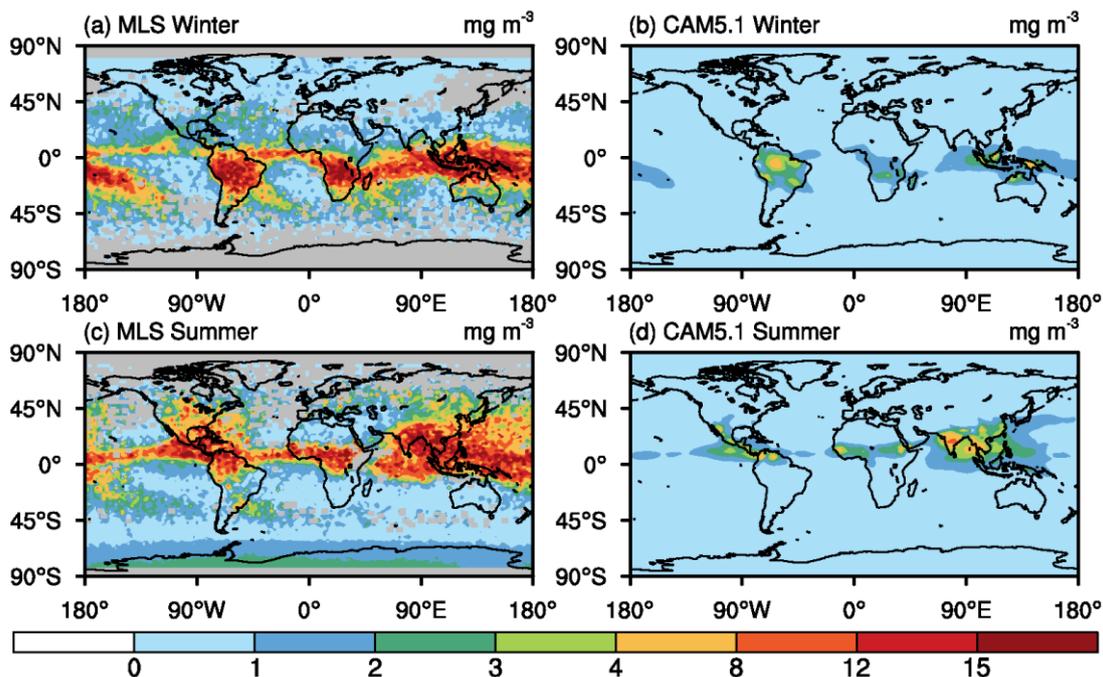
Figure R2. Comparison between (left) MLS observed and (right) CAM5.1 simulated cloud ice content (unit: mg m^{-3}) at 215 hPa during (top) winter and (bottom) summer. All results are 3-year averages for 2005–2007. Grey areas indicate where required data are not available.

(d) The comparisons of simulated convective/stratiform precipitation with the Tropical Rainfall Measuring Mission (TRMM) precipitation radar data are shown in Fig. R3. Convective and stratiform precipitations have comparable magnitudes in TRMM measurement, while the precipitation in CAM5.1 is mainly contributed by the convective precipitation parameterization (Yang et al., 2013). The partition of convective and stratiform precipitations is one of the major challenges in the current model physics (Arakawa, 2004). Dai (2006) also reported that most of the GCMs still have problems in reproducing an accurate magnitude of stratiform precipitation compared to TRMM data. However, because the CAM5.1 model can reproduce the total precipitation reasonably well, we focused on the result from the source apportionment of total precipitation in this study.
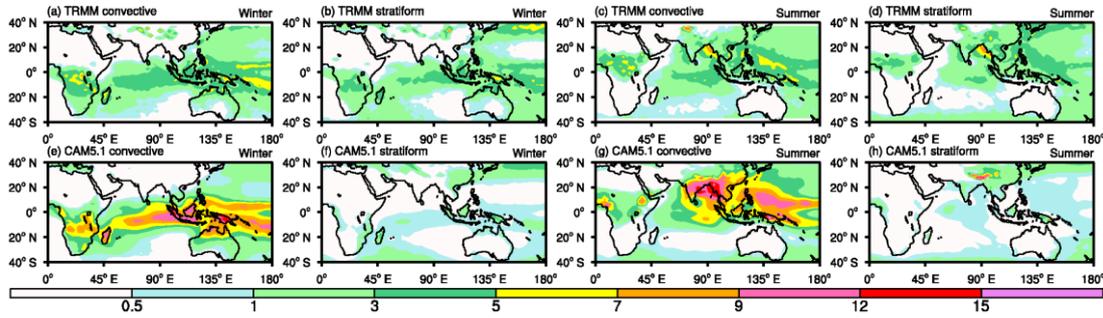
Figure R3. Comparison between (top) TRMM observed and (bottom) CAM5.1 simulated convective and stratiform precipitations (unit: mm d^{-1}) during (leftmost two columns) winter and (rightmost two columns) summer for 1998–2007.

(e) We compared the evaporation flux in CAM5.1 with data from the Objectively Analyzed Air-sea Fluxes (OAFlux) Project, as shown in Fig. R4. Overall the evaporation in CAM5.1 is in good agreement with that in OAFlux datasets. In this study, CAM5.1 is driven by MERRA data, in which the latent heat flux is computed from the evaporation flux. Meanwhile, the latent heat flux is used to calculate the surface evaporation in CAM5.1. Therefore, the evaporation flux in CAM5.1 is very close to that in MERRA. Jiménez et al. (2011) and Bosilovich et al. (2011) provided a detailed assessment on the evaporation in MERRA compared to other global estimates and observation. Thus, we cited the two papers instead of re-assessing the evaporation flux again in our manuscript. In general, the evaporation of MERRA over land is larger than the evaporation in other global estimates (Jiménez et al., 2011). Bosilovich et al. (2011) pointed out that the evaporation in MERRA is lower compared to OAFlux, while other estimates generally overestimate evaporation over oceans. In contrast, the MERRA evaporation is much closer to OAFlux data than other estimates. These biases in MERRA data may lead to the higher land contribution and lower oceanic contribution to precipitation in the results from source apportionment in this study. In the revised manuscript, we have mentioned the above discussions in the last paragraph of Sect. 3.2.
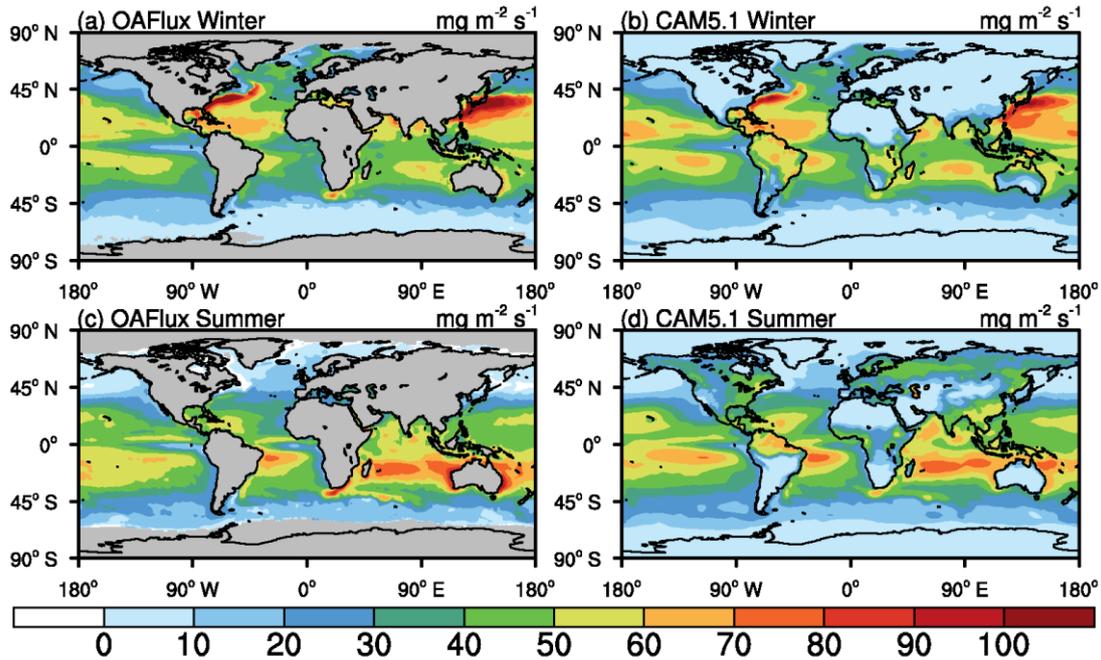
Figure R4. Distributions of the evaporation fluxes (unit: mg m^{-2} s^{-1}) in OAFlux datasets and CAM5.1 during winter and summer for 1998–2007. Grey areas indicate where required data are not available.

(f)   Here, we compared the simulated terrestrial water storage with Gravity Recovery and Climate Experiment (GRACE) observation, as shown in Fig. R5. We used the three latest land water solutions provided by GFZ, JPL, and CSR in the GRACE data. To be consistent with GRACE observation, the baseline average over 2004 to 2009 are removed in simulated results, as shown in Fig. R5a. The overall seasonal cycle of total water storage can be characterized by the model, but the amplitude in model is significantly larger than that in observations. Note that the evaporation in MERRA is used to drive the CAM5.1 model. Thus, there is no virtual moisture transmit from the Earth's surface into the atmosphere in the specified dynamics simulation of CAM5.1.
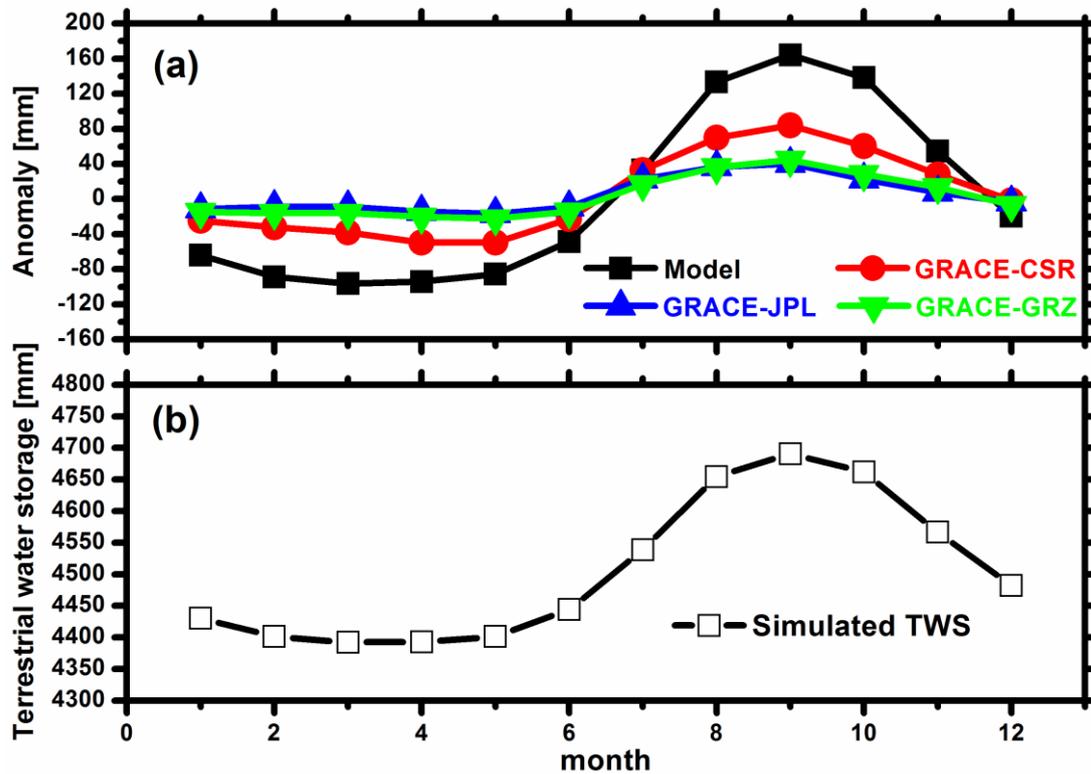
Figure R5. (a) The evolution of GRACE-derived anomaly in terrestrial water storage and that in simulated terrestrial water storage relative to the average for 2003–2009 over the land areas within $10\,°N–40\,°N$ and $60\,°E–120\,°E$. (b) The evolution of simulated terrestrial water storage.

(g)   In the revised manuscript, we have added a discussion on the assessment of the simulated horizontal wind fields. In general, the horizontal wind fields in CAM5.1 are in agreement with those from National Centers for Environmental Prediction (NCEP). Please see Sect. 3.1 in the revised manuscript and Fig. S7 in the supplementary information. A corresponding conclusion has been added in Sect. 4 in the revised manuscript.

3. In the simulation, WNP contribution in terms of percentage to YRV precipitation was the largest in cool season. This is not obvious when looking at long-term mean water moisture flux shown in Figure 3. The contribution is likely associated with the synoptic disturbances that could bring moisture from south. The authors may need to provide their views somewhere in the text. Moisture transport is likely contributed by a large portion by synoptic disturbances. But the manuscript tends to discuss the related dynamics based only on long-term mean water vapor flux.

Reply: Thank you for your suggestion. In the revised manuscript, we divided the meridional and zonal water vapour flux into stationary and transient terms. Please see supplementary Figs. S8–S9. Figure S8c shows that the transient component of the

12

meridional flux brings some of the moisture from south over most of the NWP and the north of the SCS. Figure S9c shows that the transient component of the zonal flux leads to westwards water vapour transport over 20 °–30 °N for the NWP. Both the transient components indicated that the synoptic disturbances could bring moisture originating from the NWP to the southern and eastern coastal regions of Asia during winter. We have added this view in Sect. 3.3 in the revised manuscript.

4. Contribution from each region is difficult to distinguish in the bar charts shown in Figure 6-8. Could authors re-plot bar charts by stacking all regions according to their region number (e.g., 1 to 25 from bottom to top) and present a schematic showing the stacking scheme?

Reply: Thank you for your suggestion. For Figs. 6–8, all bar charts are plotted by stacking all regions according to their region number (1 to 25 from bottom to top). We have also added legends to show the stacking scheme in the revised manuscript.

II. Tagged AWTs

1. The approaches for adding tagged water vapor and qc and qi within individual physical parameterizations need more detailed description in section 2, especially for the macrophysics and microphysics schemes. For example in macrophysics, I does not quite understand how the tagging of those microphysical, advection, and convective tendency from other processes in solving Park's matrix in the macrophysics was done. Similarly, details for those complicated microphysical processes were not discussed. Also, snow and rain (important sink of tagged water) were diagnostically determined in the microphysics of CAM5.1 version. Snow and rain are important sinks of tagged water. However, no discussion on these two hydrometeors was provided.

Reply: Thank you for your suggestion.

(a) We have added more detailed descriptions on the tagged AWTs method in Sect. 2 in the revised manuscript.

(b) In the cloud macrophysics, Park et al. (2014) defined the grid-mean net condensation rate of water vapour into liquid stratus condensate $\bar{Q}_l$ as the time change of $\bar{q}_{l,a}$ minus the external forcing (all processes except stratus macrophysics, including stratus microphysics, moisture turbulence, advection, and convection) of cloud droplets $\bar{F}_l$:

$$\bar{Q}_l = \dot{\bar{q}}_{l,a} - \bar{F}_l = A_{l,\text{st}}\dot{q}_{l,\text{st}} + \alpha q_{l,\text{st}}\dot{A}_{l,\text{st}} - \bar{F}_l \tag{R1}$$

where $\dot{\bar{q}}_{l,a}$, $\dot{q}_{l,\text{st}}$, and $\dot{A}_{l,\text{st}}$ are the time tendency of $\bar{q}_{l,a}$, $q_{l,\text{st}}$, and $A_{l,\text{st}}$ during $\Delta t = 1800$ s, respectively. In CAM5.1, $\alpha = 0.1$ is the ratio of newly formed or dissipated stratus to the preexisting $q_{l,\text{st}}$. Similarly, the tagged grid-mean net condensation rate $\bar{Q}_{l,tg}^k$ is calculated as:

$$\bar{Q}_{l,tg}^k = \dot{\bar{q}}_{l,a,tg}^k - \bar{F}_{l,tg}^k = A_{l,\text{st},tg}^k\dot{q}_{l,\text{st}} + \alpha q_{l,\text{st}}\big(R\dot{A}_{l,\text{st}} + A_{l,\text{st}}\dot{R}\big) - \bar{F}_{l,tg}^k, \text{and } R = \frac{\bar{q}_{v,tg}^k}{\sum_{k=1}^n \bar{q}_{v,tg}^k} \tag{R2}$$

13

Here, $\dot{R}$ is the tendency of R during Δt, and $\bar{F}_{l,tg}^k$ is the changes of tagged cloud droplets in processes such as microphysics, moisture turbulence, advection, and deep and shallow convections. We have added these sentences in the last paragraph of Sect. 2.3 in the revised manuscript.

(c) We have added descriptions on the calculations of tagged water substances in the microphysical processes. Please see Sect. 2.4.1–2.4.7 in the revised manuscript.

(d) We have added some descriptions on the calculations of tagged snow and tagged rain in the microphysical processes. Please see Sect. 2.4.8 in the revised manuscript.

2. How were the detrained qc and qi from deep and shallow convection schemes tagged and put into macrophysics?

Reply: Thank you for your question.

(a) In the deep convection scheme, only the detrainment of cloud water is taken into consideration. Equation (6c) of Zhang and McFarlane (1995) is used to calculate the MMR of cloud water q_l in the updraft. Finally, the detrainment of cloud water is calculated as the product of q_l and the detrainment rate. Similarly, the MMR of tagged cloud water $q_{l,tg}^k$ is calculated in the similar equation as the Eq. (6c) of Zhang and McFarlane (1995), but $q_{l,tg}^k$ is substituted for q_l. The detrainment of tagged cloud water is calculated as the product of $q_{l,tg}^k$ and the detrainment rate as well. We have stated that the calculation of the detrainment of tagged cloud water is identical to the detrainment of cloud water, but $q_{l,tg}^k$ is substituted for q_l. A similar sentence has been added in Sect. 2.1 in the revised manuscript.

(b) In the shallow scheme, because the detrainment of cloud water and ice ($D(q_l)$ and $D(q_i)$) is assumed to be proportional to the total water detrainment and the detrained air is assumed to be a representative of cumulus updraft (Park and Bretherton, 2009), we use the ratio of tagged total water in the updraft $q_{t,u,tg}^k$ and the corresponding sum to distribute the detrainment of tagged cloud water and ice ($D(q_{l,tg}^k)$ and $D(q_{i,tg}^k)$). We have explained this in Sect. 2.2 in the revised manuscript. The corresponding calculation of $q_{t,u,tg}^k$ has also been added in Sect. 2.2 in the revised manuscript.

(c) In the macrophysics, the detrainments of cumulus condensates were added to q_l and q_i, and then to compute the final equilibrium state in-stratus. Similarly, the tendencies of detrained cumulus condensates were also added, and Eqs. (13)–(19) in the revised manuscript are used to partition the equilibrium state of tagged water in-stratus.

3. How was the adjustment exactly done when the sum of tendencies of all tagged water substances was not equal to the tendency of the corresponding original substance? How big the adjustment can be? Would the results be quite different if no adjustment were done?

Reply: Thank you for your suggestion.

(a) We have rewritten the description of the adjustment. Equations (42) and (43) have also been added to express the adjustment in the revised manuscript. Please see Sect. 2.7 in the revised manuscript.

14

(b) The adjustment was used to ensure that the summed MMRs of the tagged water is brought back to the value of the standard water. We have evaluated the differences between the results with adjustment and which without adjustment. The adjustment can cause the change of 4.0–4.8 g m^{-2} for summed tagged water vapour (accounts for 0.02–0.026% of the MMR of water vapour), the change of 0.075–0.11 g m^{-2} for summed tagged cloud water (accounts for 0.14–0.19% of the MMR of cloud water), and the change of 0.15–0.57 g m^{-2} for summed tagged cloud ice (accounts for 2.8–7.7% of the MMR of cloud ice) at the global scale.

(c) If no adjustment was made, the results generally have no significant difference. As shown in Figs. R6–R8, for most of source regions, their water tracers in the calculation with the adjustment are very close to the results from the calculation without the adjustment at the global scale. For source regions such as ANC, IND, and NEA, there are differences in their contributions to water substances between the results with adjustment and which without adjustment. However, contributions from these source regions to water substances are generally small at the global scale. The adjustment has tiny effect on the result to determine the dominant source regions of atmospheric water substances.

15
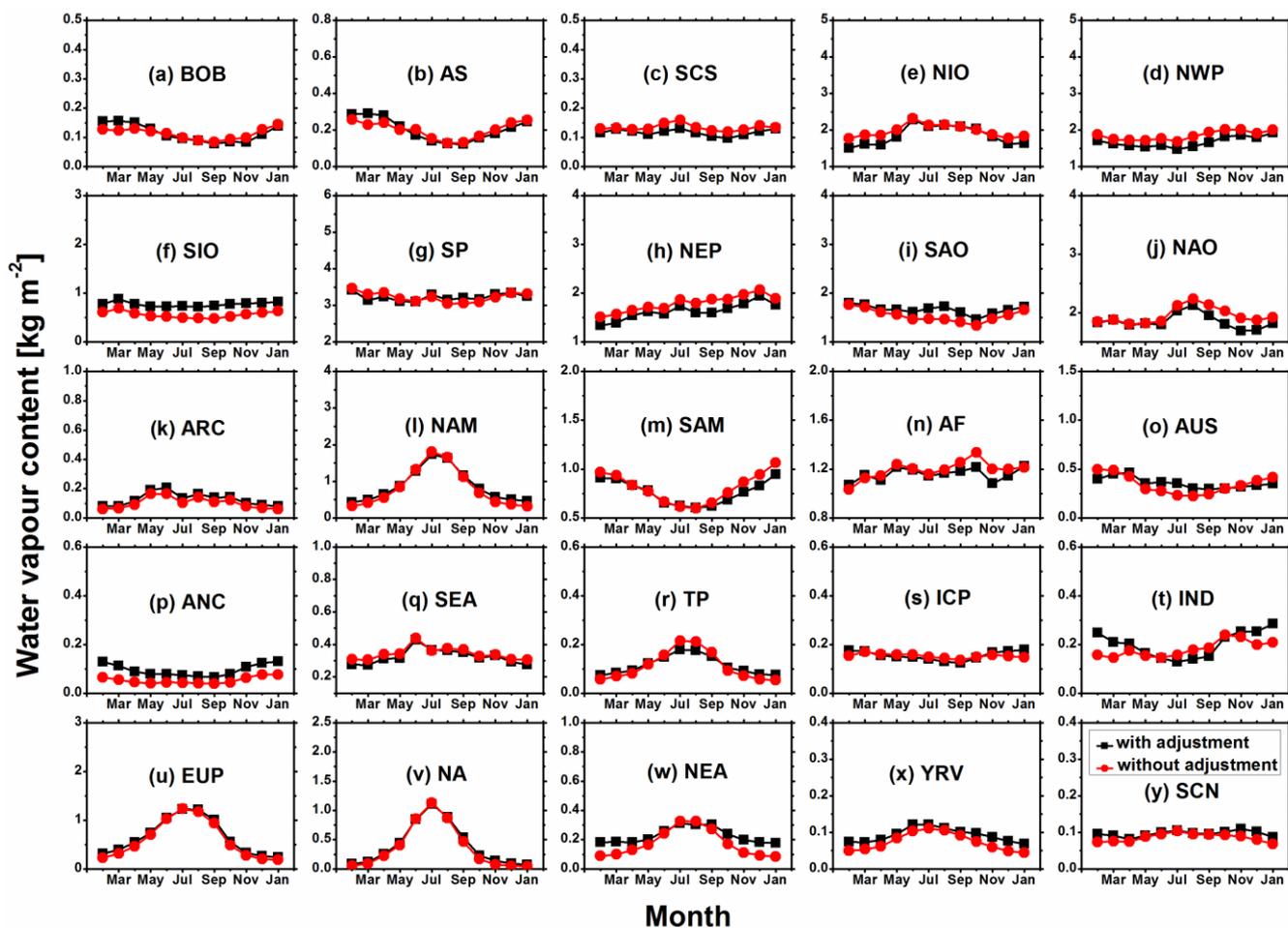
Figure R6. Comparisons between the tagged water vapour contents (unit: kg m^{-2}) in which the adjustment is applied (black) and the corresponding results with no adjustment (red) for February 1997 to January 1998. Figs. R6(a)–R6(x) correspond to the tagged water vapour originating from the source regions 1–25 defined in Fig. 1, respectively. All results are global average values.
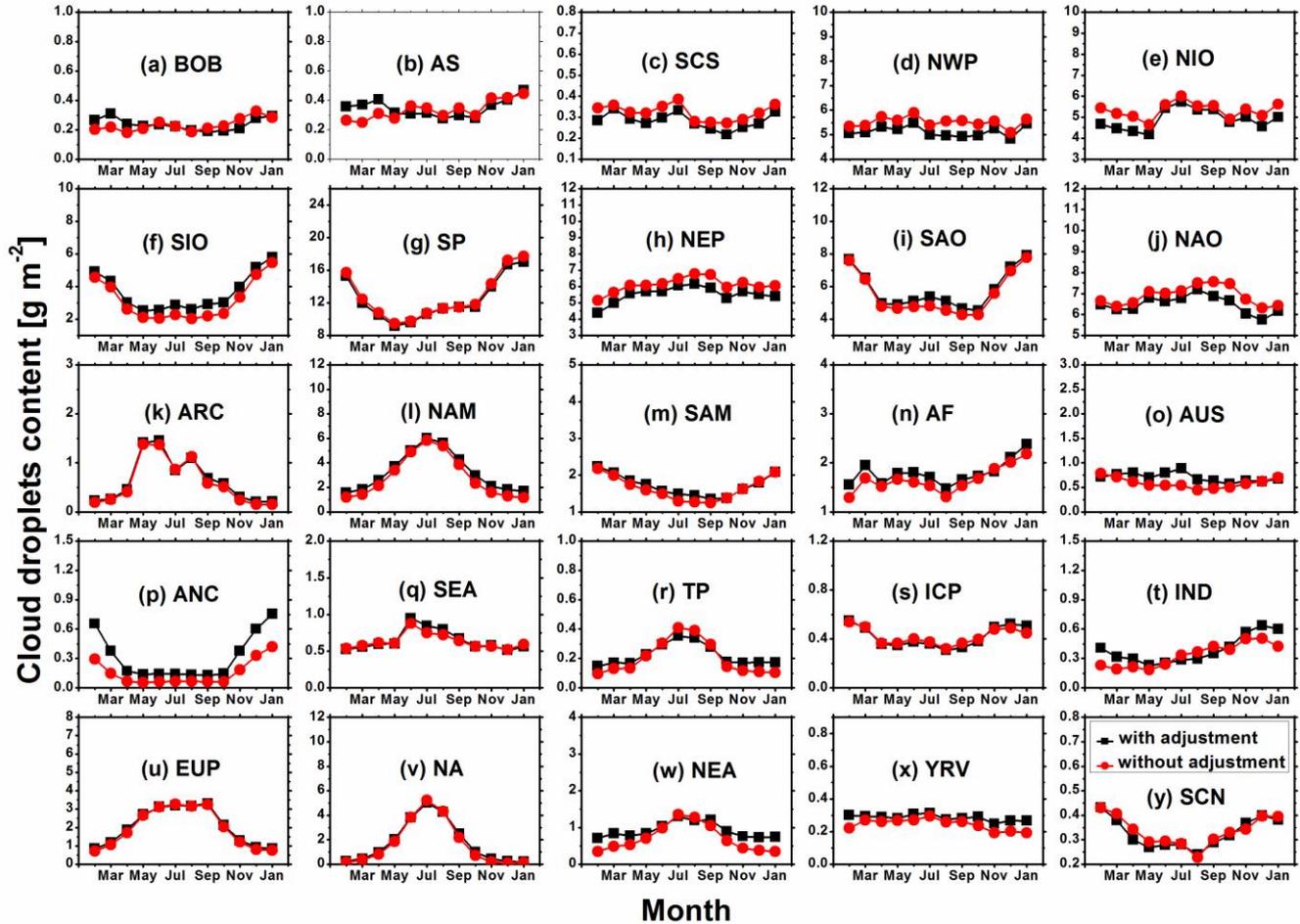
Figure R7. Same as Fig. R6, but for the tagged cloud droplets contents (unit: g m^{-2}).
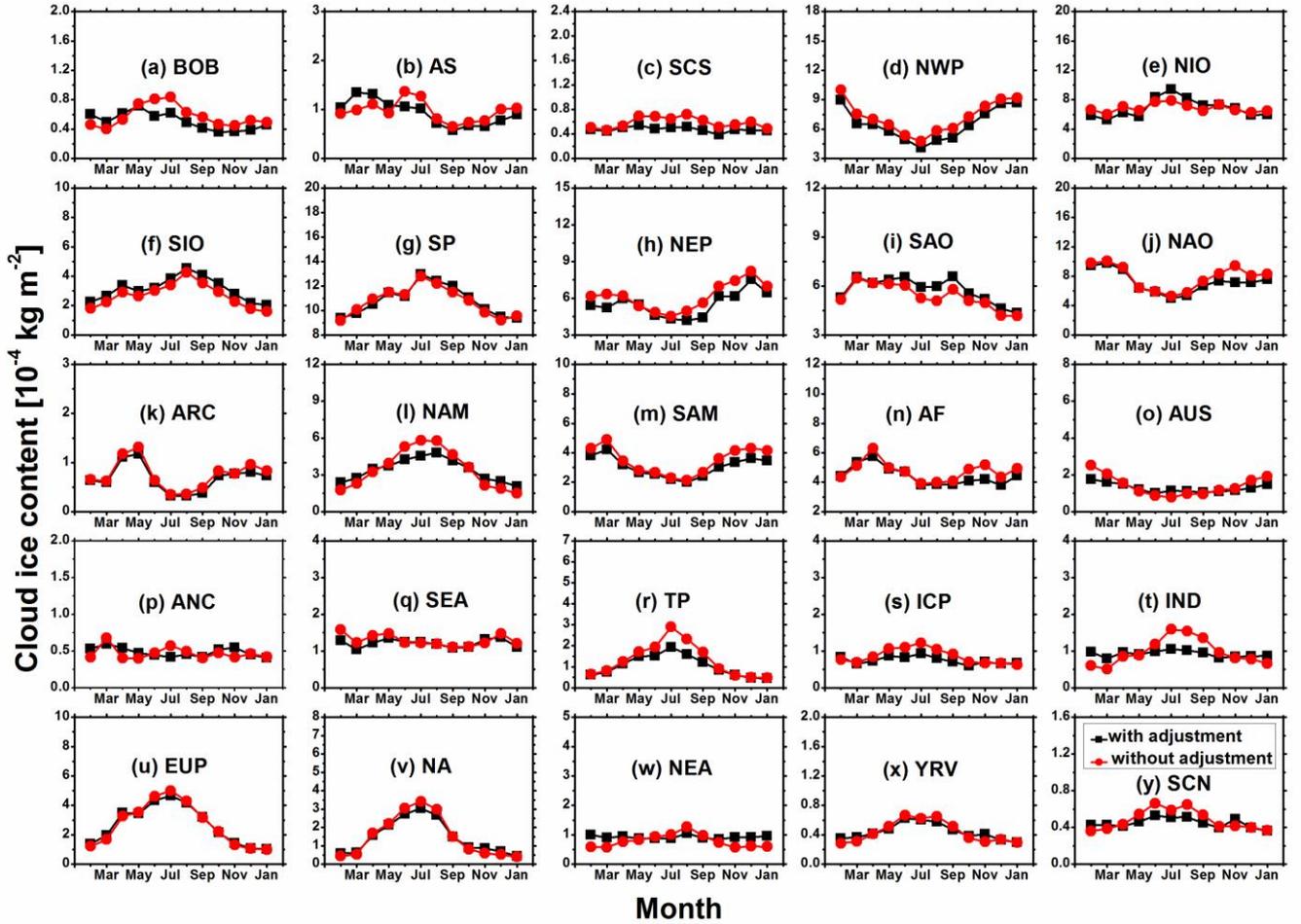
Figure R8. Same as Fig. R6, but for tagged cloud ice contents (unit: 10^{-4} kg m^{-2}).

4. In CAM5, evaporation of convective rainfall is assumed to be as Sunqvist (1988), which is proportional to the square root of the total rainwater flux at each level. Therefore, the linear partitioning of evaporation based on precipitation flux of tagged water (eq.2) does not seem to be consistent with the formulation used in the model.

Reply: The evaporation rate $\left(\frac{\partial q_v^k}{\partial t}\right)_{\text{dp\_evap}}$ at level m is associated with the deep convection precipitation flux $(Q_m)_{\text{dp}}$ at the top interface of this level (Sundqvist, 1998), expressed as

$$\left(\frac{\partial q_v^k}{\partial t}\right)_{\text{dp\_evap}} = k_e(1 - \text{RH}_m)\sqrt{(Q_m)_{\text{dp}}} \tag{R3}$$

where RH_m is the relative humidity at level m and the coefficient $k_e = 2 \times 10^{-6}$ (kg m^{-2} s^{-1})$^{-1/2}$ s^{-1}. The basic idea of the AWT method is to separate the contribution from each source region to the content of atmospheric water substances in each relevant physical process. If Eq. (R3) is used to compute the evaporation rate of tagged convection precipitation

17

$\left(\frac{\partial q_{v,tg}^k}{\partial t}\right)_{\text{dp\_evap}}$ at level m, in most cases $\sum_{k=1}^n \left(\frac{\partial q_{v,tg}^k}{\partial t}\right)_{\text{dp\_evap}} \neq k_e(1 - \text{RH}_m)\sqrt{\sum_{k=1}^n \left(Q_{m,tg}^k\right)_{\text{dp}}}$ due to the nonlinearity of Eq.

(R3). However, Eq. (R3) is equivalent to

$$\left(\frac{\partial q_v^k}{\partial t}\right)_{\text{dp\_evap}} = k_e(1 - \text{RH}_m)\frac{(Q_m)_{\text{dp}}}{\sqrt{(Q_m)_{\text{dp}}}}, \text{if } (Q_m)_{\text{dp}} \neq 0 \tag{R4}$$

Thus, if $\sum_{k=1}^n \left(Q_{m,tg}^k\right)_{\text{dp}} \neq 0$, the summed evaporation rate of tagged precipitation must satisfy the below equation:

$$\sum_{k=1}^n \left(\frac{\partial q_{v,tg}^k}{\partial t}\right)_{\text{dp\_evap}} = k_e(1 - \text{RH}_m)\frac{\sum_{k=1}^n \left(Q_{m,tg}^k\right)_{\text{dp}}}{\sqrt{\sum_{k=1}^n \left(Q_{m,tg}^k\right)_{\text{dp}}}} = k_e(1 - \text{RH}_m)\frac{\left(Q_{m,tg}^1\right)_{\text{dp}} + \left(Q_{m,tg}^2\right)_{\text{dp}} + \cdots + \left(Q_{m,tg}^n\right)_{\text{dp}}}{\sqrt{\sum_{k=1}^n \left(Q_{m,tg}^k\right)_{\text{dp}}}} \tag{R5}$$

Because Eq. (R3) reflects that there is positive correlation between the evaporation rate and precipitation flux, we assume the individual evaporation rate of tagged convection precipitation from source region k is expressed as:

$$\left(\frac{\partial q_{v,tg}^k}{\partial t}\right)_{\text{dp\_evap}} = \begin{cases} k_e(1 - \text{RH}_m)\dfrac{\left(Q_{m,tg}^k\right)_{\text{dp}}}{\sqrt{\sum_{k=1}^n \left(Q_{m,tg}^k\right)_{\text{dp}}}}, & \text{if } \sum_{k=1}^n \left(Q_{m,tg}^k\right)_{\text{dp}} \neq 0, \\ 0, & \text{if } \sum_{k=1}^n \left(Q_{m,tg}^k\right)_{\text{dp}} = 0, \end{cases} \tag{R6}$$

In addition, the evaporation rate of convection precipitation is very small compared to the tendency of water vapour in convection process, as reported by Neale et al. (2012). Equation (R6) is sufficient to partition the evaporation rate of each tagged convection precipitation.

Changes in manuscript: The corresponding descriptions have been added in Sect. 2.1 for deep convection and in Sect. 2.2 for shallow convection.

5. Some of the formulation of tagged water substance in the macrophysics are confusing, especially for the cloud fraction. How can the stratus cloud fraction be composed proportionally of each tagged condensates without mixing?

Reply: The separate liquid stratus fraction $a_{l,\text{st}}$ is a unique function of grid-mean relative humidity over water, $\bar{u}_l \equiv \bar{q}_v/\bar{q}_{s,w}$, where $\bar{q}_v$ is the grid-mean water vapour specific humidity and $\bar{q}_{s,w}$ is the grid-mean saturation specific humidity over water, which is shown in Eq. (3) of Park et al. (2014):

$$a_{l,\text{st}} = \begin{cases} 1, & \text{if } \bar{u}_l \geq \hat{u}_l, \\ 1 - \left[\frac{3}{\sqrt{2}}\left(\frac{\hat{u}_l - \bar{u}_l}{\hat{u}_l - u_{\text{cl}}}\right)\right]^{\frac{2}{3}}, & \text{if } \frac{1}{6}(5\hat{u}_l + u_{\text{cl}}) \leq \bar{u}_l \leq \hat{u}_l, \\ 4\cos\left[\frac{1}{3}\left\{\arccos\left[\frac{3}{2\sqrt{2}}\left(\frac{\hat{u}_l - \bar{u}_l}{\hat{u}_l - u_{\text{cl}}}\right)\right] - 2\pi\right\}\right]^2, & \text{if } u_{\text{cl}} \leq \bar{u}_l \leq \frac{1}{6}(5\hat{u}_l + u_{\text{cl}}), \\ 0, & \text{if } \bar{u}_l \leq u_{\text{cl}}, \end{cases} \tag{R7}$$

where in-cloud RH $\hat{u}_l = 1$. u_{cl} is the critical RH that liquid stratus starts to form and serves as a tuning parameter in CAM5.1, whose values depended on height and surface properties are presented in Park et al. (2014). Then the single-phase (no separate liquid and ice phases) liquid stratus fraction is

$$A_{l,\text{st}} = (1 - A_{\text{cu}})a_{l,\text{st}} \tag{R8}$$

Here A_{cu} is the total cumulus fraction.

Equation (R7) is a complicated nonlinear function of $\bar{u}_l$, and it is difficult to separately extract the individual tagged liquid stratus fraction. $A_{l,st}$ is a monotone increasing function of $\bar{u}_l$: the larger MMR of grid-mean tagged water vapour $\bar{q}_{v,tg}^k$, the more contribution to $A_{l,st}$ from the source region k. All the tagged water substances from the source region are assumed to have the identical physical properties and be well-mixed. Thus, we simply allocate the tagged single-phase liquid stratus fraction $A_{l,st,tg}^k$, which depends on the ratio of $\bar{q}_{v,tg}^k$ and the corresponding sum and is expressed as:

$$A_{l,st,tg}^k = \left(\frac{\bar{q}_{v,tg}^k}{\sum_{k=1}^n \bar{q}_{v,tg}^k}\right) A_{l,st} \tag{R9}$$

The tagged grid-mean liquid stratus condensate $\bar{q}_{l,a,tg}^k$ is calculated in the same way as the grid-mean liquid stratus condensate $\bar{q}_{l,a}$, but $A_{l,st,tg}^k$ is substituted for $A_{l,st}$:

$$\bar{q}_{l,a,tg}^k = A_{l,st,tg}^k \times q_{l,st} \tag{R10}$$

Here, $q_{l,st}$ is the in-stratus liquid water content (LWC).

Similar to $a_{l,st}$, the separate ice stratus fraction $a_{i,st}$ is a function of the grid-mean total ice RH over ice, $\bar{v}_i \equiv (\bar{q}_v + \bar{q}_i)/\bar{q}_{s,i}$, where $\bar{q}_i$ is the MMR of grid-mean ice and $\bar{q}_{s,i}$ is the grid-mean saturation specific humidity over ice, as shown in Eq. (4) of Park et al. (2014):

$$a_{i,st} = \left(\frac{\bar{v}_i - u_{ci}}{\hat{u}_i - u_{ci}}\right)^2 \tag{R11}$$

where the in-cloud RH over ice $\hat{u}_i = 1.1$, and the critical RH that ice stratus begins to form $u_{ci} = 0.80$ in CAM5.1. Similar to $A_{l,st}$, the single-phase ice stratus fraction is calculated as

$$A_{i,st} = (1 - A_{cu})a_{i,st} \tag{R12}$$

As in the treatment of $A_{l,st,tg}^k$, the tagged ice stratus fraction $A_{i,st,tg}^k$ is computed based on the ratio of grid-mean total tagged ice specific humidity $(\bar{q}_{v,tg}^k + \bar{q}_{i,tg}^k)$ and the corresponding sum since the nonlinearity of the calculation in $a_{i,st}$, expressed as

$$A_{i,st,tg}^k = \left[\frac{(\bar{q}_{v,tg}^k + \bar{q}_{i,tg}^k)}{\sum_{k=1}^n (\bar{q}_{v,tg}^k + \bar{q}_{i,tg}^k)}\right] A_{i,st} \tag{R13}$$

The tagged grid-mean ice stratus condensate $\bar{q}_{i,a,tg}^k$ is calculated in the same way as the grid-mean ice stratus condensate $\bar{q}_{i,a}$:

$$\bar{q}_{i,a,tg}^k = A_{i,st,tg}^k \times q_{i,st} \tag{R14}$$

Here, $q_{i,st}$ is the in-stratus IWC. Using the same formula as for the calculation of the grid-mean ambient water vapour specific humidity, the tagged grid-mean ambient water vapour specific humidity $\bar{q}_{v,a,tg}^k$ is computed as follows:

$$\bar{q}_{v,a,tg}^k = \bar{q}_{v,tg}^k + \bar{q}_{l,tg}^k + \bar{q}_{i,tg}^k - \bar{q}_{l,a,tg}^k - \bar{q}_{i,a,tg}^k \tag{R15}$$

Though the tagged cloud fractions were assumed to be composed proportionally of each tagged water vapour specific humidity and the grid-mean total tagged ice specific humidity, the summed tendencies of tagged water substances are very close to the corresponding tendencies of original water substances in most of grid points in cloud processes when the adjustment in Sect. 2.7 is not applied (see Fig. S3). Figure S6 also shows that the summed MMRs of tagged water substances are approximated to the MMRs of original water substances in most of grid points. In addition, our results on the

contributions of evaporations from land, the North Atlantic Ocean, extended north Indian Ocean, and extended Northwest Pacific to precipitation over Eurasia are close to the results of Numaguti (1999). In the future, we will find a more exact way to partition the tagged cloud fraction.

Changes in manuscript: The corresponding descriptions of tagged water substance in the macrophysics have been added in Sect. 2.3 in the revised manuscript.

Minor comments:

1. It is "Neale et al." rather than "Neal et al." in the text (line 99).

Reply: Thank you for your suggestion. We have modified this citation in the revised manuscript.

2. It is "Gettelman" rather than "Gettleman" in the text (line 189, 190, 196).

Reply: Thank you for your suggestion. We have modified these citations in the revised manuscript.

3. It is not clear what Figure S7-S10 exactly show. To where and what the vapour tracers supplied from 25 source regions contribute?

Reply: Thank you for your suggestion. We have rewritten the captions of these figures (Figs. S10–S13) in the supplement of the revised manuscript. Figures S10 and S11 show the contribution of tagged water vapour tracer from each moisture source region defined in Fig. 1 to water vapour content over Eurasia and its surrounding areas in winter and summer, respectively. Figures S12 and S13 show the contribution of tagged precipitation from each moisture source region defined in Fig. 1 to precipitation over Eurasia and its surrounding areas in winter and summer, respectively.

Changes in manuscript: Please see Lines 48–50, Lines 52–54, Lines 56–57, and Lines 59–60 in the supplement of the revised manuscript.

Relevant references added in this response:

Arakawa, A.: The cumulus parameterization problem: Past, present, and future, J. Climate, 17(13), 2493–2525, doi:10.1175/1520-0442(2004)017<2493:RATCPP>2.0.CO;2, 2004.

Dai, A.: Precipitation characteristics in eighteen coupled climate models, J. Climate, 19(18), 4605–4630, doi:10.1175/JCLI3884.1., 2006.

Waliser, D. E., Li, J. L. F., Woods, C. P., Austin, R. T., Bacmeister, J., Chern, J., Genio, A. D., Jiang, J. H., Kuang, Z., Meng, H., Minnis, P., Platnick, S., Rossow, W. B., Stephens, G. L., Sun-Mack, S., Tao, W.-K., Tompkins, A. M., Vane, D. G.,

Walker, C., and Wu, D.: Cloud ice: A climate model challenge with signs and expectations of progress, J. Geophys. Res. Atmos., 114(D8), doi:10.1029/2008JD010015, 2009.

Yang, B., Qian, Y., Lin, G., Leung, L. R., Rasch, P. J., Zhang, G. J., McFarlane, S. A., Zhao, C., Zhang, Y., Wang, H., Wang, M., and Liu, X.: Uncertainty quantification and parameter tuning in the CAM5 Zhang-McFarlane convection scheme and impact of improved convection on the global circulation and climate, J. Geophys. Res. Atmos., 118(2), 395–415, doi:10.1029/2012JD018213, 2013.

Source apportionment of atmospheric water over East Asia – a source tracer study in CAM5.1

Chen Pan[1], Bin Zhu[1], Jinhui Gao[1], Hanqing Kang[1]

[1]Key Laboratory of Meteorological Disaster, Ministry of Education (KLME), Joint International Research Laboratory of Climate and Environment Change (ILCEC), Collaborative Innovation Center on Forecast and Evaluation of Meteorological Disasters, Key Laboratory for Aerosol-Cloud-Precipitation of China Meteorological Administration, Nanjing University of Information Science & Technology, Nanjing, 210044, China

Correspondence to: Bin Zhu (binzhu@nuist.edu.cn)

9 **Abstract**

10 The atmospheric water tracer (AWT) method is implemented in the Community Atmosphere Model version 5.1 (CAM5.1)

11 to quantitatively identify the contributions of various source regions to precipitation and water vapour over East Asia.

12 Compared to other source apportionment methods, the AWT method was developed based on detailed physical

13 parameterizations, and can therefore trace the behaviour of atmospheric water substances directly and exactly. According to

14 the simulation, the north Indian Ocean (NIO) is the dominant oceanic moisture source region for precipitation over the

15 Yangtze River Valley (YRV) and South China (SCN) in summer, while the Northwest Pacific (NWP) dominates during

16 other seasons. Evaporation over the South China Sea (SCS) is responsible for only 2.87–4.23.7% of summer precipitation

17 over the YRV and SCN. In addition, the Indo-China Peninsula is an important terrestrial moisture source region (annual

18 contribution of ~10%). The overall relative contribution of each source region to the water vapour amount is similar to the

19 corresponding contribution to precipitation over the YRV and SCN. A case study for the SCS shows that only a small part

20 (≤5.85%) of water vapour originates from local evaporation, while much more water vapour is supplied by the NWP and

21 NIO. In addition, because evaporation from the SCS represents only a small contribution to the water vapour over the YRV

22 and SCN in summer, the SCS mainly acts as a water vapour transport pathway where moisture from the NIO and NWP meet.

23

1 Introduction

Water vapour is <u>one of</u> the most important component<u>s</u> of the atmosphere, affecting global climate and weather patterns (Held and Soden, 2000). Among current studies of the hydrological cycle, the identification of moisture sources to the atmosphere is an important topic, because a better understanding of these sources will benefit long-term forecasting, disaster prevention<u>,</u> and allocation of water resources (Bosilovich and Schubert, 2002).

Source apportionment methods have been developed to identify atmospheric moisture source regions. These methods generally can be divided into three types, namely analytical models, isotopes<u>,</u> and numerical (Lagrangian and Eulerian) atmospheric water tracers (AWTs) (Gimeno et al., 2012). In addition, sensitivity experiments in numerical simulations such as shutting down water vapour flux at the lateral boundaries or surface evaporation (Chow et al., 2008) are an approach to study the contributions of moisture from diverse regions. Analytical models, widely used in earlier studies (Brubaker et al., 1993; Burde and Zangvil, 2001; Eltahir and Bras, 1996; Savenije, 1995; Trenberth, 1999), are generally based on various simplifying assumptions such as a well-mixed atmosphere. The stable isotopes of water, HDO and $H_2^{18}O$, can be used to investigate the water cycle. However, water isotope data reflect a series of processes that occur simultaneously, which makes it difficult to interpret isotope results for the water cycle (Numaguti, 1999; Sodemann and Zubler, 2010). The Lagrangian method has become a popular way to analyse the transport of moisture and moisture sources of precipitation (Dirmeyer and Brubaker, 1999; Gustafsson et al., 2010; Sodemann et al., 2008; Stohl and James, 2004; Stohl et al., 2008). However, Gimeno et al. (2012) pointed out that the treatments of water vapour transport and changes of atmospheric water vapour in the Lagrangian method are not based on detailed physical equations. Sodemann and Zubler (2010) pointed out that a strong bias exists in Lagrangian precipitation estimates, because all cloud processes are neglected. Sensitivity experiments generally contain nonlinearities, which may lead to changes in the dynamic and thermodynamic structures of meteorological fields, suggesting that their results cannot be used to directly diagnose moisture sources. In contrast, the Eulerian AWT method has been developed based on detailed physical parameterizations in atmospheric models, enabling a direct and exact tracking of the behaviour of atmospheric water substances (Numaguti, 1999; Bosilovich, 2002).

50

51   The Eulerian AWT method was firstly developed by Joussaume et al. (1986) and Koster et al. (1986) for global circulation

52   models (GCMs). Later, this AWT method was applied to diagnose regional water sources in GCMs. For example, Numaguti

53   (1999) identified the moisture sources of Eurasian precipitation, and Bosilovich and Schubert (2002) diagnosed the moisture

54   sources of precipitation over North America and India. Bosilovich et al. (2003) studied water sources of the large-scale

55   North American monsoon, Bosilovich (2002) investigated the vertical distribution of water vapour tracers over North

56   America, and Sodemann et al. (2009) used this method to study sources of water vapour leading to a flood event in Central

57   Europe using a mesoscale model. Finally, Knoche and Kunstmann (2013) incorporated the AWT method into a fifth-

58   generation mesoscale model to study the transport of atmospheric moisture in West Africa.

59

60   In summer, the Asian summer monsoon (ASM) brings large amounts of water vapour to the East Asian (EA) continent,

61   leading to a wet season and abundant precipitation. Simmonds et al. (1999) pointed out that the dominant moisture transport

62   pathways during summer can be divided into three branches, namely (i) southwesterly flow associated with the Indian

63   summer monsoon, (ii) southerly or southeasterly flow associated with the southeastern Asian monsoon, and (iii) the mid-

64   latitude Westerlies. Correspondingly, these pathways transport moisture from (i) the Bay of Bengal (BOB) and the Arabian

65   Sea (AS), (ii) the South China Sea (SCS) and the Northwest Pacific (NWP), and (iii) the mid-latitude regions. Simmonds et

66   al. (1999) and Xu et al. (2008) pointed out that the BOB to SCS are the main source regions for rainfall over southeast China.

67   Using the Lagrangian Flexible Particle (FLEXPART) dispersion model (Stohl and James, 2004), Drumond et al. (2011)

68   discovered that the inland regions of China receive moisture mostly from western Asia, while the East China Sea (ECS) and

69   SCS are the main source regions for rainfall in China's eastern and southeastern coastal areas and the AS and BOB are the

70   main source regions for southern and central China from April to September. With the FLEXPART model, Baker et al.

71   (2015) demonstrated that the Indian Ocean is the primary source of moisture for East Asian summer monsoon (EASM)

72   rainfall. Using the same model, Chen et al. (2013) suggested that the ECS, the SCS, the Indian peninsula and BOB, and the

73   AS were the four major moisture source regions for summer water vapour over the Yangtze River Valley (YRV) during

74   2004–2009. Chow et al. (2008) suggested that water vapour supplied by the Indian summer monsoon contributed about 50%

75 to early summer precipitation over China in 1998, and inferred that the SCS may act as a pathway for water vapour transport

76 affected by the Indian and Southeast Asian summer monsoon. However, recently Wei et al. (2012), using a Lagrangian

77 model, showed that the major moisture transport pathways to the YRV are over land and not over the ocean. Therefore, the

78 dominant source regions of moisture for summer rainfall over EA are still uncertain.

79

80 Baker et al. (2015) pointed out that the water vapour transport mechanisms for precipitation over China during the ASM are

81 still unquantified. Previous studies have pointed out that analytical models need simplifying assumptions, isotope data ~~not~~

82 ~~only~~ reflects more than just the water cycle, the Lagrangian methods lack cloud processes, and ~~that~~ sensitivity experiments

83 contain nonlinearities, limiting diagnostic studies of moisture sources. On the other hand, the Eulerian AWT method does

84 not have these shortcomings and is an accurate way to quantitatively determine water sources (Bosilovich, 2002). Therefore,

85 in this study, we aim at incorporating an Eulerian AWT approach into an advanced global atmosphere model – the

86 Community Atmosphere Model version 5.1 (CAM5.1) (Neale et al., 2012). Using this method, we address the following

87 questions: (1) What moisture source regions are most important for precipitation and water vapour amount over EA,

88 including the YRV and South China (SCN)? (2) What is the role of the SCS for precipitation and water vapour amount over

89 EA during the EASM: a dominant source region or just a pathway for water vapour transport from other source regions?

90

91 In this study, detailed descriptions of physical parameterization schemes and means of implementing the AWT mechanisms

92 in CAM5.1 are given in Sect. 2. Simulation results, including evaluation and discussion, are presented in Sect. 3. Finally,

93 summary and concluding remarks are presented in Sect. 4.

94

95 **2 Model and methods**

96 The CAM5.1, released by the U.S. National Center for Atmospheric Research, is the atmospheric component of the

97 Community Earth System Model (CESM) (Neale et al., 2012). Compared to CAM4, CAM5.1 contains a range of

98 improvements in the representation of physical processes such as moist turbulence, shallow convection, stratiform

99 microphysics, cloud macrophysics schemes, and others (Neale et al., 2012). The horizontal resolution used in this study is

100 1.9 °in latitude and 2.5 °in longitude. The vertical range is from the surface to approximately 4 hPa (≈ 40 km).

101

102 In this study, the chemistry mechanism of CAM5.1 is taken from MOZART-4 (Emmons et al., 2010), in which water vapour

103 is invariant, which means that it is unnecessary to consider changes in water vapour during chemical processes. The basic

104 simulations setup, including emissions and upper and lower boundary conditions, is identical to that of the specified

105 dynamics simulations of CAM5 in Lamarque et al. (2012). In this study, the wet removal scheme is taken fromin Horowitz

106 et al. (2003) is adopted. The temporal evolution of the mass mixing ratios (MMRs) of different water substances (water

107 vapour, cloud droplets, and ice) is determined by deep convection, shallow convection, cloud macrophysics, cloud

108 microphysics, advection, and vertical diffusion. To diagnose the dominant moisture source regions of atmospheric water

109 over EA, the global surface is divided into 25 source regions as shown in Fig. 1. Most regions are defined based on the

110 locations of continents and oceans. Due to the focus on moisture sources over EA in this study, EA and its adjacent regions

111 are further divided to provide more detail. Within source region k, the surface flux of the tagged water vapour tracer E^k is

112 equal to the surface evaporation flux of water vapour E; otherwise $E^k = 0$. As in the treatment described in Knoche and

113 Kunstmann (2013) and Bosilovich and Schubert (2002), water is "tagged" when it evaporates at its source region and is no

114 longer tagged when it precipitates from the atmosphere to the Earth's surface via atmospheric processes. When previously

115 tagged precipitation reevaporates from the surface, it is regarded as newly tagged water (Knoche and Kunstmann, 2013),

116 which then belongs to the region from where it reevaporates.

117

118 The MMRs of water vapour, cloud droplets, and ice at a particular level are defined as q_v, q_l, and q_i, respectively. The

119 corresponding MMRs of tagged water substances from source region k are $q_{v,tg}^k$, $q_{l,tg}^k$, and $q_{i,tg}^k$. We assume that all the

120 tagged water substances from the source regions have the identical physical properties and are well-mixed. All these tagged

121 water substances are passive, which means that they are entirely separate from the original water substances in CAM5.1 and

122 have no impact on dynamical and thermal fields. Numaguti (1999) suggested that the lifetime of atmospheric water vapour is

123 about 10 days. In this study, the simulation is started in 01 January 1997, and the initial MMRs of tagged substances are set

124   to zero. To attain stable initial concentrations of tagged water substances, the simulation experiment takes a year to spin up.

125   We then investigate the ten-year averaged results for 1998 to 2007. In the following, we describe the treatment of tagged

126   AWTs in CAM5.1's physical parameterizations.

127

128   **2.1 Deep convection**

129   In CAM5.1, deep convection is parameterized using the approach described in Zhang and McFarlane (1995), but with

130   modifications following Richter and Rasch (2008) and Raymond and Blyth (1986, 1992). For the temporal evolution of $q_{v,tg}^k$,

131   it is calculated in the same way as that of q_v, but the relevant variables of tagged water vapour are substituted for the

132   corresponding variables of original water vapour, In the calculation of consistent transport of deep convection, we assume the

133   ratio of tagged and original water vapour tendencies, respectively denoted as $\left(\frac{\partial q_{v,tg}^k}{\partial t}\right)_{dp}$ and $\left(\frac{\partial q_v}{\partial t}\right)_{dp}$, is equal to the ratio of

134   the relevant tagged water vapour MMR and the corresponding sum, expressed as:

135    $$\left(\frac{\partial q_{v,tg}^k}{\partial t}\right)_{dp} = \frac{q_{v,tg}^k}{\sum_{k=1}^n q_{v,tg}^k} \times \left(\frac{\partial q_v}{\partial t}\right)_{dp} \tag{1}$$

136    $$\left(\frac{\partial q_{v,tg}^k}{\partial t}\right)_{dp} = \epsilon_{tg}^k - c_{tg}^k - \frac{1}{\rho}\frac{\partial}{\partial z}\left(M_{u,dp} q_{v,u,tg}^k + M_{d,dp} q_{v,d,tg}^k - M_{c,dp} q_{v,tg}^k\right) \tag{1}$$

137   where $M_{c,dp}$ is the net vertical mass flux, $M_{u,dp}$ is the upward mass flux, and $M_{d,dp}$ is the downward mass flux in the deep

138   convection. ϵ_{tg}^k and c_{tg}^k are the large-scale mean evaporation and condensation rates of tagged water vapour, respectively.

139   Here, $q_{v,u,tg}^k$ and $q_{v,d,tg}^k$ are the MMR of tagged water vapour in the updraft and that in the downdraft, respectively. The ratio

140   between the MMR of tagged water vapour and the corresponding sum is used to calculate the condensation rate c_{tg}^k:

141    $$c_{tg}^k = \left(\frac{q_{v,tg}^k}{\sum_{k=1}^n q_{v,tg}^k}\right) c \tag{2}$$

142   where c is the condensation of original water vapour. In this study, n=25, which is the total number of defined source regions

143   (Fig. 1). In this scheme, the tagged cloud water in the updraft, the detrainment of tagged cloud water, rain production rate,

144   and the evaporation rate of tagged rain in the downdraft are calculated in the same ways manner as that for the corresponding

28

145 quantities for original water~~;. but~~However, the relevant variables of tagged water vapour are substituted for the

146 corresponding variables of original water vapour. ~~The d~~Detailed formulas ~~to~~for ~~the~~ relevant quantities for original water in

147 the updraft and downdraft are ~~described~~presented in ~~the~~ Sect. 3 of Zhang and McFarlane (1995).~~the assumed ratio~~

148 ~~relationship in Eq. (1) is also used to calculate the production of tagged cloud water in updraft, as well as the tagged rain~~

149 ~~production rate and evaporation rate of tagged rain in downdraft.~~ The evaporation of convection precipitation is also

150 considered in this parameterization.

151 The evaporation rate $\left(\frac{\partial q_v^k}{\partial t}\right)_{\text{dp\_evap}}$ at level m is associated with the deep convection precipitation flux $(Q_m)_{\text{dp}}$ at the top

152 interface of this level (Sundqvist, 1998), express~~ing~~ed as

153
$$\left(\frac{\partial q_v^k}{\partial t}\right)_{\text{dp\_evap}} = k_e(1-\text{RH}_m)\sqrt{(Q_m)_{\text{dp}}} \tag{3}$$

154 where RH_m is the relative humidity at level m and the coefficient $k_e = 2 \times 10^{-6}$ (kg m^{-2} s^{-1})$^{-1/2}$ s^{-1}. ~~We assume t~~The

155 individual evaporation rate of tagged convection precipitation from source region k is calculated as:

156
$$\left(\frac{\partial q_{v,tg}^k}{\partial t}\right)_{\text{dp\_evap}} = \begin{cases} k_e(1-\text{RH}_m)\dfrac{\left(Q_{m,tg}^k\right)_{\text{dp}}}{\sqrt{\sum_{k=1}^n \left(Q_{m,tg}^k\right)_{\text{dp}}}}, & \text{if } \sum_{k=1}^n \left(Q_{m,tg}^k\right)_{\text{dp}} \neq 0, \\ 0, & \text{if } \sum_{k=1}^n \left(Q_{m,tg}^k\right)_{\text{dp}} = 0 \end{cases} \tag{4}$$

157 In general~~ly~~, the evaporation rate of convection precipitation is very small compared to the tendency of water vapour in the

158 deep convection (Neale et al., 2012).~~Because the evaporation rate is associated with the deep convection precipitation flux~~

159 ~~Q_{dp}, we use the ratio of the tagged deep convection precipitation flux $Q_{dp,tg}^k$ and the corresponding sum to calculate the~~

160 ~~evaporation of tagged deep convection precipitation:~~

161
$$\left(\frac{\partial q_{v,tg}^k}{\partial t}\right)_{\text{dp\_evap}} = \frac{Q_{dp,tg}^k}{\sum_{k=1}^n Q_{dp,tg}^k} \times \left(\frac{\partial q_v}{\partial t}\right)_{\text{dp\_evap}} \tag{2}$$

162 For the temporal evolution of $q_{l,tg}^k$ and $q_{i,tg}^k$ in the deep convection parameterization, both are treated in the same

163 subroutine as q_l and q_i.

164

2.2 Shallow convection

The shallow convection scheme in CAM5.1 is taken from Park and Bretherton (2009). ~~Like~~Similar to the MMR of the total water q_t, the MMR of the tagged total water $q_{t,tg}^k$ is also assumed to be a conserved quantity in non-precipitating moist adiabatic processes. In this scheme, the diagnostic equations for the shallow convective mass flux $M_{u,\text{sh}}$ and the MMR of the updraft total water $q_{t,u}$ (Bretherton et al., 2004) are expressed as:

$$\frac{\partial M_{u,\text{sh}}}{\partial z} = E_{tr} - D_{tr} \qquad (5)$$

and

$$\frac{\partial}{\partial z}\left(q_{t,u} M_{u,\text{sh}}\right) = E_{tr}\bar{q}_t - D_{tr} q_{t,u} + \left(\frac{\partial q_t}{\partial z}\right) M_{u,\text{sh}} \qquad (6)$$

where E_{tr} is the entrainment rate, D_{tr} is the detrainment rate, and $\bar{q}_t$ is the MMR of the mean environmental total water. The fractional entrainment and detrainment rates are denoted as ε and δ, then

$$E_{tr} = \varepsilon M_{u,\text{sh}}, D_{tr} = \delta M_{u,\text{sh}} \qquad (7)$$

Finally, attaining the updraft dilution equations:

$$\frac{\partial M_{u,\text{sh}}}{\partial z} = M_{u,\text{sh}}(\varepsilon - \delta) \qquad (8)$$

$$\frac{\partial q_{t,u}}{\partial z} = \varepsilon(\bar{q}_t - q_{t,u}) + \frac{\partial q_t}{\partial z} \qquad (9)$$

Similarly, the updraft dilution equation for the tagged total water is expressed as:

$$\frac{\partial q_{t,u,tg}^k}{\partial z} = \varepsilon(\bar{q}_{t,tg}^k - q_{t,u,tg}^k) + \frac{\partial q_{t,tg}^k}{\partial z} \qquad (10)$$

~~The Eq.~~Equation (A5) of Bretherton et al. (2004) is used to calculate $q_{t,u}$, as well as $q_{t,u,tg}^k$, in the shallow convection. In this scheme, because the detrainment of cloud water and ice ($D(q_l)$ and $D(q_i)$) is assumed to be proportional to the total water detrainment and the detrained air is assumed to be a representative of cumulus updraft (Park and Bretherton, 2009), we use the ratio of tagged total water in the updraft $q_{t,u,tg}^k$ and the corresponding sum to distribute the detrainment of tagged cloud water and ice ($D(q_{l,tg}^k)$ and $D(q_{i,tg}^k)$):

$$D\left(q_{l,tg}^k\right) = \left(\frac{q_{t,u,tg}^k}{\sum_{k=1}^{n} q_{t,u,tg}^k}\right) \times D(q_l), \; D\left(q_{i,tg}^k\right) = \left(\frac{q_{t,u,tg}^k}{\sum_{k=1}^{n} q_{t,u,tg}^k}\right) \times D(q_i) \qquad (11\text{3})$$

187 This ratio is also applied to the calculations of in-cumulus tagged condensates and the production rates of tagged rain/snow

188 by cumulus expulsion of condensates to the environment. Tagged condensate tendencies for compensating subsidence or

189 upwelling, the tagged condensate tendencies due to detrained cloud water and ice without precipitation contribution, and the

190 updraft/penetrative entrainment mass flux of tagged total water are calculated ~~with~~using the same equations ~~as~~for the original

191 water-related quantities in this scheme. ~~Like~~Similar to the calculation of the tendency of water vapour, the tendency of

192 tagged water vapour is computed as the difference between the tendency of tagged total water and the tendencies of tagged

193 condensates in non-precipitating processes within the shallow convection scheme. ~~Like CAM5.1's deep convection scheme,~~

194 ~~t~~The shallow convection scheme relates precipitation evaporation rate $\left(\frac{\partial q_v}{\partial t}\right)_{\text{sh\_evap}}$ to shallow convection precipitation flux

195 Q_{sh}, similar to the deep convection scheme of CAM5.1. Therefore, we use an assumed expression ~~such as~~~~like~~similar to Eq.

196 (~~2~~4) to calculate the tagged precipitation evaporation rate at a level m:

197
$$\left(\frac{\partial q_{v,tg}^{k}}{\partial t}\right)_{\text{sh\_evap}} = \begin{cases} k_e(1-\text{RH}_m)\dfrac{\left(Q_{m,tg}^{k}\right)_{\text{sh}}}{\sqrt{\sum_{k=1}^{n}\left(Q_{m,tg}^{k}\right)_{\text{sh}}}}, & \text{if } \sum_{k=1}^{n}\left(Q_{m,tg}^{k}\right)_{\text{sh}} \neq 0 \\ 0, & \text{if } \sum_{k=1}^{n}\left(Q_{m,tg}^{k}\right)_{\text{sh}} = 0 \end{cases} \tag{12}$$

198 where $\left(Q_{m,tg}^{k}\right)_{\text{sh}}$ is the tagged precipitation flux at the top interface of level m.

199 ~~$\left(\frac{\partial q_{v,tg}^{k}}{\partial t}\right)_{\text{sh\_evap}} = \frac{Q_{sh,tg}^{k}}{\sum_{k=1}^{n}Q_{sh,tg}^{k}} \times \left(\frac{\partial q_v}{\partial t}\right)_{\text{sh\_evap}}$~~ ~~(4)~~

200 ~~Tagged condensate tendencies for compensating subsidence or upwelling and penetrative entrainment mass flux are~~

201 ~~calculated with the same equations as the original water-related quantities in this scheme.~~

202

2.3 Cloud Macrophysics

204 Park et al. (2014) provided a detailed description of CAM5.1's cloud macrophysics, in which cloud fractions, horizontal and

205 vertical overlapping structures of clouds, and net condensation rates of water vapour into cloud droplets and ice are

206 computed. Because the tendencies of water substances caused by cumulus convection have been calculated in deep and

207 shallow convection schemes, we focus on the treatment of the tagged stratus fraction and net condensation rates of tagged

208 water vapour in stratus clouds in this section.

209

210 The separate liquid stratus fraction $a_{l,\text{st}}$ is a unique function of grid-mean relative humidity (RH) over water, $\bar{u}_l \equiv \bar{q}_v/\bar{q}_{s,w}$

211 $\bar{u}_t = \bar{q}_v/\bar{q}_{s,w}$, where $\bar{q}_v$ is the grid-mean water vapour specific humidity and $\bar{q}_{s,w}$ is the grid-mean saturation specific

212 humidity over water, which is shown in Eq. (3) of Park et al. (2014). Then the single-phase (no separate liquid and ice phases)

213 liquid stratus fraction is

214 $A_{l,\text{st}} = (1 - A_{\text{cu}})a_{l,\text{st}}$ (13)

215 Here A_{cu} is the total cumulus fraction.

216 We allocate the tagged liquid stratus fraction $A_{l,\text{st},tg}^k$, which depends on the ratio of grid-mean tagged water vapour specific

217 humidity $\bar{q}_{v,tg}^k$ and the corresponding sum, expressed as:

218 $A_{l,\text{st},tg}^k = \left(\dfrac{\bar{q}_{v,tg}^k}{\sum_{k=1}^n \bar{q}_{v,tg}^k}\right) A_{l,\text{st}} \dfrac{\bar{q}_{v,tg}^k}{\sum_{k=1}^n \bar{q}_{v,tg}^k} \times A_{l,\text{st}}$

219 (14) (5)

220 The tagged grid-mean liquid stratus condensate $\bar{q}_{l,\text{a},tg}^k$ is calculated in the same way as the grid-mean liquid stratus

221 condensate $\bar{q}_{l,\text{a}}$, but $A_{l,\text{st},tg}^k$ is substituted for $A_{l,\text{st}}$:

222 $\bar{q}_{l,\text{a},tg}^k = A_{l,\text{st},tg}^k \times q_{l,\text{st}}$ (15)

223 Here, $q_{l,\text{st}}$ is the in-stratus liquid water content (LWC). This ratio is also used in the computation of tagged in-stratus liquid

224 water content (LWC) $q_{l,\text{st},tg}^k$ and tagged grid-mean ambient LWC $\bar{q}_{l,\text{a},tg}^k$, thus

225 $q_{l,\text{st},tg}^k = \dfrac{\bar{q}_{v,tg}^k}{\sum_{k=1}^n \bar{q}_{v,tg}^k} \times q_{l,\text{st}}$ (6)

226 and

227 $\bar{q}_{l,\text{a},tg}^k = \dfrac{\bar{q}_{v,tg}^k}{\sum_{k=1}^n \bar{q}_{v,tg}^k} \times \bar{q}_{l,\text{a}}$ (7)

Here, $q_{l,st}$ is the in-stratus LWC and $\overline{q_{l,a}}$ is the grid-mean ambient LWC. Similar to $Aa_{l,\mathrm{st}}$, the ice stratus fraction $Aa_{i,\mathrm{st}}$ is a

function of the grid-mean total ice RH over ice, $\bar{v}_i \equiv (\bar{q}_v + \bar{q}_i)/\bar{q}_{s,i} \overline{v_t \equiv (q_v + q_i)/q_{s,i}}$, where $\bar{q}_i \overline{q_t}$ is the grid-mean ice

specific humidity and $\bar{q}_{s,i} \overline{q_{s,i}}$ is the grid-mean saturation specific humidity over ice, as shown in Eq. (4) of Park et al. (2014).

Similar to $A_{l,\mathrm{st}}$, the single-phase ice stratus fraction is calculated as

$$A_{i,\mathrm{st}} = (1 - A_{\mathrm{cu}})a_{i,\mathrm{st}} \tag{16}$$

~~Like~~As in the treatment of $A_{l,\mathrm{st},tg}^{k}$, the tagged ice stratus fraction $A_{i,\mathrm{st},tg}^{k}$ is computed based on the ratio of grid-mean total

tagged ice specific humidity $(\bar{q}_{v,tg}^{k} + \bar{q}_{i,tg}^{k})$ and the corresponding sum:

$$A_{i,\mathrm{st},tg}^{k} = \left[\frac{(\bar{q}_{v,tg}^{k} + \bar{q}_{i,tg}^{k})}{\sum_{k=1}^{n}(\bar{q}_{v,tg}^{k} + \bar{q}_{i,tg}^{k})} \right] A_{i,\mathrm{st}} \tag{17}$$

The tagged grid-mean ice stratus condensate $\bar{q}_{i,a,tg}^{k}$ is calculated in the same way as the grid-mean ice stratus condensate $\bar{q}_{i,a}$:

$$\bar{q}_{i,a,tg}^{k} = A_{i,\mathrm{st},tg}^{k} \times q_{i,\mathrm{st}} \tag{18}$$

Here, $q_{i,\mathrm{st}}$ is the in-stratus ice water content (IWC). ~~Therefore, the tagged ice stratus fraction $A_{i,st,tg}^{k}$, tagged in-stratus ice~~

~~water content (IWC) $q_{i,st,tg}^{k}$ and subsequent tagged grid-mean ambient IWC $\overline{q_{i,a,tg}^{k}}$ are all calculated based on the ratio of~~

~~grid-mean total tagged ice specific humidity $(\overline{q_{v,tg}^{k}} + \overline{q_{i,tg}^{k}})$ and the corresponding sum, expressed as:~~

$$\overline{A_{i,st,tg}^{k} = \frac{(\overline{q_{v,tg}^{k}} + \overline{q_{i,tg}^{k}})}{\sum_{k=1}^{n}(q_{v,tg}^{k} + q_{i,tg}^{k})} \times A_{i,st}} \tag{8}$$

$$\overline{q_{i,st,tg}^{k} = \frac{(\overline{q_{v,tg}^{k}} + \overline{q_{i,tg}^{k}})}{\sum_{k=1}^{n}(q_{v,tg}^{k} + q_{i,tg}^{k})} \times q_{i,st}} \tag{9}$$

$$\overline{q_{i,a,tg}^{k}} = \frac{(\overline{q_{v,tg}^{k}} + \overline{q_{i,tg}^{k}})}{\sum_{k=1}^{n}(q_{v,tg}^{k} + q_{i,tg}^{k})} \times \overline{q_{i,a}} \tag{10}$$

~~Here, $q_{i,st}$ is the in-stratus IWC and $\overline{q_{i,a}}$ is the grid-mean ambient IWC.~~ Using the same formula as for the calculation of the

grid-mean ambient water vapour specific humidity, the tagged grid-mean ambient water vapour specific humidity

$\bar{q}_{v,a,tg}^{k} \overline{q_{v,a,tg}^{k}}$ is computed as follows:

$$\bar{q}_{v,a,tg}^{k} = \bar{q}_{v,tg}^{k} + \bar{q}_{l,tg}^{k} + \bar{q}_{i,tg}^{k} - \bar{q}_{l,a,tg}^{k} - \bar{q}_{i,a,tg}^{k} \quad \overline{q_{v,a,tg}^{k}} = \overline{q_{v,tg}^{k}} + \overline{q_{l,tg}^{k}} + \overline{q_{i,tg}^{k}} - \overline{q_{l,a,tg}^{k}} - \overline{q_{i,a,tg}^{k}}$$

$$\tag{19~~1~~}$$

250 In CAM5.1, Park et al. (2014) defined the grid-mean net condensation rate of water vapour into liquid stratus condensate $\bar{Q}_l$

251 as the time change of $\bar{q}_{l,a}$ minus the external forcing (all processes except stratus macrophysics, including stratus

252 microphysics, moisture turbulence, advection, and convection) of cloud droplets $\bar{F}_l$:

253 $$\bar{Q}_l = \dot{\bar{q}}_{l,a} - \bar{F}_l = A_{l,\mathrm{st}}\dot{q}_{l,\mathrm{st}} + \alpha q_{l,\mathrm{st}}\dot{A}_{l,\mathrm{st}} - \bar{F}_l \hspace{2cm} (20)$$

254 where $\dot{\bar{q}}_{l,a}$, $\dot{q}_{l,\mathrm{st}}$, and $\dot{A}_{l,\mathrm{st}}$ are the time tendency of $\bar{q}_{l,a}$, $q_{l,\mathrm{st}}$, and $A_{l,\mathrm{st}}$ during $\Delta t = 1800$ s, respectively. In CAM5.1, $\alpha = 0.1$

255 is the ratio of newly formed or dissipated stratus to the preexisting $q_{l,\mathrm{st}}$. Similarly, the tagged grid-mean net condensation

256 rate $\bar{Q}_{l,tg}^k$ is calculated as:

257 $$\bar{Q}_{l,tg}^k = \dot{\bar{q}}_{l,a,tg}^k - \bar{F}_{l,tg}^k = A_{l,\mathrm{st},tg}^k \dot{q}_{l,\mathrm{st}} + \alpha q_{l,\mathrm{st}}\left(R\dot{A}_{l,\mathrm{st}} + A_{l,\mathrm{st}}\dot{R}\right) - \bar{F}_{l,tg}^k, \text{ and } R = \frac{\bar{q}_{v,tg}^k}{\sum_{k=1}^{n}\bar{q}_{v,tg}^k} \hspace{1cm} (21)$$

258 Here, $\dot{R}$ is the tendency of R during Δt, and $\bar{F}_{l,tg}^k$ is the changes of tagged cloud droplets in processes such as microphysics,

259 moisture turbulence, advection, and deep and shallow convections.

2.4 Cloud Microphysics

262 The CAM5.1 model uses the double-moment cloud microphysical scheme described in Morrison and ~~Gettleman~~ Gettelman

263 (2008) and a modified treatment of ice supersaturation and ice nucleation from ~~Gettleman~~ Gettelman et al. (2010). In

264 addition, CAM5.1's stratus microphysics is formulated using a single-phase stratus fraction A_{st}, which is assumed as the

265 maximum overlap between $A_{l,\mathrm{st}}$ and $A_{i,\mathrm{st}}$ (Park et al., 2014). In this study, the same assumption is applied to each tagged

266 single-phase stratus fraction $A_{\mathrm{st},tg}^k$. The microphysical processes in CAM5.1 include condensation/deposition,

267 evaporation/sublimation, autoconversion of cloud droplets and ice to form rain and snow, accretion of cloud droplets and ice

268 by rain or by snow, heterogeneous freezing, homogeneous freezing, melting, sedimentation, activation of cloud droplets, and

269 primary ice nucleation. Detailed formulations for these microphysical processes are described in Morrison and ~~Gettleman~~

270 Gettelman (2008).

271 ~~For processes such as condensation/deposition of cloud water and ice, evaporation/sublimation of cloud water and ice,~~

272 ~~conversion of cloud water to rain, conversion of cloud ice to snow, accretion of cloud water and ice, freezing of cloud water~~

273 ~~and ice and ice nucleation, the calculations of the tendencies of water substances can be regarded as terms multiplied by the~~

274 ~~stratus fraction. Therefore, the corresponding tendencies of tagged water substances are computed by multiplication by the~~

275 ~~tagged stratus fraction, while the remaining terms in the formulations remain unchanged. For calculations of melting of~~

276 ~~cloud ice and snow, evaporation/sublimation of precipitation and sedimentation of cloud water and ice, the tendencies of~~

277 ~~tagged water substances are computed using the same equations as for the original water substances but tagged variables are~~

278 ~~substituted for the original variables of the water substances. For the calculation of the tendency of activated cloud~~

279 ~~condensation nuclei, we assume that the ratio of the tendency of the tagged cloud droplets and the tendency of the original~~

280 ~~cloud droplets is equal to the ratio of $A_{i,st,tg}^k$ and the corresponding sum $\sum_{k=1}^n A_{i,st,tg}^k$.~~

281 **2.4.1 Condensation/deposition and evaporation/sublimation of cloud water and ice**

282 In CAM5.1, the net grid-mean evaporation/condensation rate of cloud water and ice (condensation minus evaporation) Q is

283 calculated following Zhang et al. (2003). In this microphysics scheme, the total grid-scale condensation rates of tagged ice

284 and tagged cloud water, as well as the total grid-scale evaporation rates of tagged cloud water and tagged ice, are calculated

285 ~~in~~using the same formulas but the tagged variables are substituted for the corresponding original variables:

286 $$\left(\frac{\partial q_{i,tg}^k}{\partial t}\right)_{\text{cond}} = \min\left[A_{\text{st},tg}^k A, A_{\text{st},tg}^k Q + \frac{q_{i,tg}^k}{\Delta t}\right], Q > 0 \qquad (22)$$

287 and

288 $$\left(\frac{\partial q_{l,tg}^k}{\partial t}\right)_{\text{cond}} = \max\left[A_{\text{st},tg}^k Q - \left(\frac{\partial q_{i,tg}^k}{\partial t}\right)_{\text{cond}}, 0\right], Q > 0 \qquad (23)$$

289 and

290 $$\left(\frac{\partial q_{l,tg}^k}{\partial t}\right)_{\text{evap}} = \max\left(A_{\text{st},tg}^k, -\frac{q_{l,tg}^k}{\Delta t}\right), Q < 0 \qquad (24)$$

291 and

292 $$\left(\frac{\partial q_{i,tg}^k}{\partial t}\right)_{\text{evap}} = \max\left[A_{\text{st},tg}^k Q - \left(\frac{\partial q_{l,tg}^k}{\partial t}\right)_{\text{evap}}, -\frac{q_{i,tg}^k}{\Delta t}\right], Q < 0 \qquad (25)$$

where A is the in-cloud deposition rate of water vapor onto cloud ice (see Eq. (21) of Morrison and Gettelman, 2008).

2.4.2 Conversion of cloud water to rain and conversion of cloud ice to snow

The grid-mean autoconversion and accretion rates of water cloud in CAM5.1 are expressed in the Eqs. (27) and (28) of Morrison and Gettelman (2008). Both the two rates can be regard as a term multiply by A_{st}. Therefore, the grid-mean autoconversion and accretion rates of tagged water cloud can be calculated in the same formula but $A_{st,tg}^{k}$ is substituted for A_{st}:

$$\left(\frac{\partial q_{l,tg}^{k}}{\partial t}\right)_{auto} = \frac{A_{st,tg}^{k}}{A_{st}}\left(\frac{\partial q_{l}}{\partial t}\right)_{auto} = -\left(\frac{\partial q_{r,tg}^{k}}{\partial t}\right)_{auto} \tag{26}$$

and

$$\left(\frac{\partial q_{l,tg}^{k}}{\partial t}\right)_{accr} = \frac{A_{st,tg}^{k}}{A_{st}}\left(\frac{\partial q_{l}}{\partial t}\right)_{accr} = -\left(\frac{\partial q_{r,tg}^{k}}{\partial t}\right)_{accw} \tag{27}$$

where $q_{r,tg}^{k}$ is the MMR of tagged stratiform rain.

Similarly, the grid-mean autoconversion rate of ice to form snow can be looked as a term multiply by A_{st} (see Eq. (29) of Morrison and Gettelman (2008)), as well as the accretion of ice followed Lin et al. (1983). Thus, the autoconversion and accretion rates of tagged ice to form snow are expressed as

$$\left(\frac{\partial q_{i,tg}^{k}}{\partial t}\right)_{auto} = \frac{A_{st,tg}^{k}}{A_{st}}\left(\frac{\partial q_{i}}{\partial t}\right)_{auto} = -\left(\frac{\partial q_{s,tg}^{k}}{\partial t}\right)_{auto} \tag{28}$$

and

$$\left(\frac{\partial q_{i,tg}^{k}}{\partial t}\right)_{accs} = \frac{A_{st,tg}^{k}}{A_{st}}\left(\frac{\partial q_{i}}{\partial t}\right)_{accs} = -\left(\frac{\partial q_{s,tg}^{k}}{\partial t}\right)_{acci} \tag{29}$$

where $q_{s,tg}^{k}$ is the MMR of tagged stratiform snow.

2.4.3 Other collection processes

The accretion of cloud water by snow $\left(\frac{\partial q_l}{\partial t}\right)_{\text{accs}} = -\left(\frac{\partial q_s}{\partial t}\right)_{\text{accw}}$ is attained by the continuous collection equation, whose collection efficiency is a function of the Stokes number following Thompson et al. (2004). ~~Like~~Similar to the calculation of $\left(\frac{\partial q_l}{\partial t}\right)_{\text{auto}}$, $\left(\frac{\partial q_l}{\partial t}\right)_{\text{accs}}$ can be regarded as a term multiply by $A_{l,\text{st}}$. Thus, $\left(\frac{\partial q_{l,tg}^k}{\partial t}\right)_{\text{accs}}$ is computed ~~in~~using the same equation but by multiplying ~~by~~with $A_{l,\text{st},tg}^k$ instead of $A_{l,\text{st}}$:

$$\left(\frac{\partial q_{l,tg}^k}{\partial t}\right)_{\text{accs}} = \frac{A_{l,\text{st},tg}^k}{A_{l,\text{st}}}\left(\frac{\partial q_l}{\partial t}\right)_{\text{accs}} = -\left(\frac{\partial q_{s,tg}^k}{\partial t}\right)_{\text{accw}} \tag{30}$$

The collection of rain by snow $\left(\frac{\partial q_r}{\partial t}\right)_{\text{coll}} = -\left(\frac{\partial q_s}{\partial t}\right)_{\text{coll}}$ can also be regarded as a term multipl~~y~~ied by A_{st}. Therefore, $\left(\frac{\partial q_{r,tg}^k}{\partial t}\right)_{\text{coll}}$ is computed ~~in~~using the same formula but by multiplying ~~by~~with $A_{\text{st},tg}^k$ instead of A_{st}:

$$\left(\frac{\partial q_{r,tg}^k}{\partial t}\right)_{\text{coll}} = \frac{A_{\text{st},tg}^k}{A_{\text{st}}}\left(\frac{\partial q_r}{\partial t}\right)_{\text{coll}} = -\left(\frac{\partial q_{s,tg}^k}{\partial t}\right)_{\text{coll}} \tag{31}$$

2.4.4 Freezing of cloud water and rain

The heterogeneous freezing of cloud water and rain is considered in CAM5.1 (Reisner et al., 1998; Morrison ~~et al.~~and Pinto, 2005). The heterogeneous freezing of tagged cloud water is computed ~~in~~using the same formula as that of original cloud water, but by multiplying ~~by~~with $A_{l,\text{st},tg}^k$ instead of $A_{l,\text{st}}$:

$$\left(\frac{\partial q_{l,tg}^k}{\partial t}\right)_{\text{het}} = \frac{A_{l,\text{st},tg}^k}{A_{l,\text{st}}}\left(\frac{\partial q_l}{\partial t}\right)_{\text{het}} \tag{32}$$

Similarly, the heterogeneous freezing of tagged rain is computed ~~in~~using the same formula as that of original rain, but by multiplying ~~by~~with $A_{\text{st},tg}^k$ instead of A_{st}:

$$\left(\frac{\partial q_{r,tg}^k}{\partial t}\right)_{\text{het}} = \frac{A_{\text{st},tg}^k}{A_{\text{st}}}\left(\frac{\partial q_r}{\partial t}\right)_{\text{het}} \tag{33}$$

The homogeneous freezing of tagged cloud droplets and tagged rain are computed ~~in~~using the same equations as those of the

original cloud droplets and rain, but $q_{l,tg}^k$ and $S_{r,tot,tg}^k$ (the vertical integrated tagged rain source/sink term) are substituted for

the original quantities:

$$\left(\frac{\partial q_{l,tg}^k}{\partial t}\right)_{\text{hom}} = \frac{\left(\frac{\partial q_l}{\partial t}\right)_{\text{hom}}}{\left(\frac{q_l}{\Delta t}\right)} \left(\frac{q_{l,tg}^k}{\Delta t}\right) = -\left(\frac{\partial q_{i,tg}^k}{\partial t}\right)_{\text{hom}} \qquad (34)$$

$$\left(\frac{\partial q_{r,tg}^k}{\partial t}\right)_{\text{hom}} = \frac{\left(\frac{\partial q_r}{\partial t}\right)_{\text{hom}}}{S_{r,tot}} S_{r,tot,tg}^k = -\left(\frac{\partial q_{s,tg}^k}{\partial t}\right)_{\text{hom}} \qquad (35)$$

2.4.5 Melting of cloud ice and snow

Similar to the calculations of the homogeneous freezing of cloud water and rain, the melting of tagged ice and tagged snow

are computed ~~in~~using the same equations as those of the original ice and snow, but $q_{i,tg}^k$ and $S_{s,tot,tg}^k$ (the vertical integrated

tagged snow source/sink term) are substituted for the original quantities:

$$\left(\frac{\partial q_{i,tg}^k}{\partial t}\right)_{\text{melt}} = \frac{\left(\frac{\partial q_i}{\partial t}\right)_{\text{melt}}}{\left(\frac{q_i}{\Delta t}\right)} \left(\frac{q_{i,tg}^k}{\Delta t}\right) = -\left(\frac{\partial q_{l,tg}^k}{\partial t}\right)_{\text{melt}} \qquad (36)$$

$$\left(\frac{\partial q_{s,tg}^k}{\partial t}\right)_{\text{melt}} = \frac{\left(\frac{\partial q_s}{\partial t}\right)_{\text{melt}}}{S_{s,tot}} \times S_{s,tot,tg}^k = -\left(\frac{\partial q_{r,tg}^k}{\partial t}\right)_{\text{melt}} \qquad (37)$$

2.4.6 Evaporation/sublimation of precipitation

For the calculations of the evaporation of tagged rain and the sublimation of tagged snow, both them are calculated ~~in~~using

the same formula as original quantities but $A_{\text{st},tg}^k$ is substituted for A_{st}:

$$\left(\frac{\partial q_{r,tg}^k}{\partial t}\right)_{\text{evap}} = \frac{A_{\text{st},tg}^k}{A_{\text{st}}} \left(\frac{\partial q_r}{\partial t}\right)_{\text{evap}} \qquad (38)$$

and

$$\left(\frac{\partial q_{s,tg}^k}{\partial t}\right)_{\text{evap}} = \frac{A_{\text{st},tg}^k}{A_{\text{st}}}\left(\frac{\partial q_s}{\partial t}\right)_{\text{evap}} \qquad\qquad (39)$$

2.4.7 Sedimentation of cloud water and ice

The time tendencies ($\left(\frac{\partial q_l}{\partial t}\right)_{\text{sed}}$ and $\left(\frac{\partial q_i}{\partial t}\right)_{\text{sed}}$) of cloud water and ice for sedimentation, as well as those ($\left(\frac{\partial q_{l,tg}^k}{\partial t}\right)_{\text{sed}}$ and

$\left(\frac{\partial q_{l,tg}^k}{\partial t}\right)_{\text{sed}}$) of tagged cloud water and tagged ice, are calculated with a simple forward differencing scheme in the vertical

dimension (Morrison and Gettelman, 2008). In CAM5.1, the sedimentation of cloud water and ice can lead to evaporation or

sublimation when the cloud fraction at the level above is larger than the cloud fraction at the given level and the evaporation

or condensation rate is assumed to be proportional to the difference in cloud fraction between the levels. This assumption is

also applied to calculate the evaporation of tagged cloud water or sublimation of tagged ice, when the tagged cloud fraction

at the level above is larger than the tagged cloud fraction at the given level.

2.4.8 The diagnosis of precipitation

The grid-scale time tendency of the MMR of precipitation q_p in CAM5.1's microphysics is expressed as:

$$\frac{\partial q_p}{\partial t} = \frac{1}{\rho}\frac{\partial(V_q\rho q_p)}{\partial z} + S_q \qquad\qquad (40)$$

where z is height, V_q is the mass-weighted terminal fall speeds (see Eq. (18) of Morrison and Gettelman (2008)), and S_q is

the grid-mean source/sink terms for q_p:

$$S_q = \left(\frac{\partial q_p}{\partial t}\right)_{\text{auto}} + \left(\frac{\partial q_p}{\partial t}\right)_{\text{accw}} + \left(\frac{\partial q_p}{\partial t}\right)_{\text{acci}} + \left(\frac{\partial q_p}{\partial t}\right)_{\text{het}} + \left(\frac{\partial q_p}{\partial t}\right)_{\text{hom}} + \left(\frac{\partial q_p}{\partial t}\right)_{\text{melt}} + \left(\frac{\partial q_p}{\partial t}\right)_{\text{evap}} + \left(\frac{\partial q_p}{\partial t}\right)_{\text{coll}} \qquad (41)$$

For the diagnostic treatments of tagged rain and tagged snow, the q_p in Eqs. (40) and (41) is replaced by $q_{r,tg}^k$ and $q_{s,tg}^k$,

respectively.

2.5 Advection

The finite volume dynamical core is chosen in this study due to its excellent properties for tracer transport (Rasch et al., 2006). The CAM5.1 model can be driven by offline meteorological fields (Lamarque et al., 2012) following the procedure initially developed for the Model of Atmospheric Transport and Chemistry (MARCH) (Rasch et al., 1997). This procedure allows for more accurate comparisons between measurements of atmospheric composition and CAM5.1's output (Lamarque et al., 2012). In this study, the external meteorological fields are obtained from Modern Era Retrospective-analysis for Research and Applications (MERRA) datasets (Rienecker et al., 2011), whose horizontal resolution is identical to CAM5.1's and time resolution is 6 h. In the simulation procedure, the zonal and meridional wind components, air temperature, surface pressure, surface temperature, surface geopotential, surface stress, and sensible and latent heat fluxes are read from the MERRA datasets to drive CAM5.1 (Lamarque et al., 2012). To prevent jumps, all input fields are linearly interpolated at timesteps between the reading times. And lLater, these fields are used to drive the CAM5.1's parameterizations to generate the necessary variables toand calculate subgrid scale transport and the hydrological cycle (Lamarque et al., 2012). Temporal evolutions of $q_{v,tg}^k$, $q_{l,tg}^k$, and $q_{i,tg}^k$ in the advective process are treated in the same manner as other constituents without any modification.

2.6 Vertical diffusion

CAM5.1's moist turbulence scheme is taken from the scheme presented by Bretherton and Park (2009), which calculates the vertical transport of heat, moisture, horizontal momentum, and tracers by symmetric turbulences. The vertical diffusion of tagged water substances is treated by the procedure in the same way as other constituents without any modification.

2.7 Adjustment

Ideally, the differences between the MMRs of water substances and the summed MMRs of all corresponding tagged water substances should be zero. However, there are exceptional differences in a few grid points (see supplementary Fig. S6). In

393　the supplement,Supplementary Figs. S1–S5 show comparisons between the tendencies of the original water substances and

394　the sum of the tendencies of the tagged water substances for the relevant physical processes described in Sects. 2.1 through

395　2.6. Although differences are small for most grid points, some abnormal values still appear randomly. For tagged water

396　vapour, evident biases mainly occur in deep convection, cloud processes (cloud macrophysics and microphysics), and

397　advection in the tropics; for tagged cloud droplets, the apparent biases generally occur in cloud processes in the tropics; for

398　tagged cloud ice, the main differences occur in cloud processes, advection, and vertical diffusion. Nonlinearities in the

399　calculations of the tendencies of water substances in the physical schemes cause these differences. A bias occurred in one

400　physical parameterization can affect the calculations of the tendencies of tagged water substances in other parameterizations,

401　since there are interactions among various physical and dynamical processes in CAM5.1. Eventually, evidentlyclear

402　differences between the summed MMRs of tagged water substances and the MMRs of original water substances may occur,

403　as shown in Fig. S6. To reduce these accumulated biases in the relevant physical schemes, additional criteria are applied to

404　the relevant quantities of the tagged water substances:

405　(1) If the positive or negative sign of the tendency of a tagged water substance is identical to the sign of the tendency of the

406　　original water substance, the absolute value of the tendency of the tagged water substance should not be larger than that

407　　of the original water substance. If their signs are different, the tendency of the tagged water substance is set to zero. This

408　　adjustment can be expressed as:

409
$$
\frac{\partial q_{tg}^{k}}{\partial t} = \begin{cases} \max\left(\frac{\partial q_{tg}^{k}}{\partial t}, \frac{\partial q}{\partial t}\right), & \text{if } \frac{\partial q_{tg}^{k}}{\partial t} \geq 0 \text{ and } \frac{\partial q}{\partial t} \geq 0 \\ \min\left(\frac{\partial q_{tg}^{k}}{\partial t}, \frac{\partial q}{\partial t}\right), & \text{if } \frac{\partial q_{tg}^{k}}{\partial t} \leq 0 \text{ and } \frac{\partial q}{\partial t} < 0 \\ 0, & \text{if } \left(\frac{\partial q_{tg}^{k}}{\partial t} < 0 \text{ and } \frac{\partial q}{\partial t} \geq 0\right) \text{ or } \left(\frac{\partial q_{tg}^{k}}{\partial t} > 0 \text{ and } \frac{\partial q}{\partial t} < 0\right) \end{cases}
\tag{42}
$$

410　　where $\frac{\partial q_{tg}^{k}}{\partial t}$ and $\frac{\partial q}{\partial t}$ represent the tendency of the tagged water substances and the tendency of the corresponding original

411　　water substance in a given physical process, respectively.

412　(2) After the adjustment in Eq. (42) being applied, theThe sum of the tendencies of all tagged water substances should be

413　　equal to the tendency of the corresponding original water substance in each scheme. This adjustment can be described as

414　　follows:

41

415
$$\frac{\partial q_{tg}^k}{\partial t} = \begin{cases} R_q \left(\frac{\partial q_{tg}^k}{\partial t} \right), & \text{if } \sum_{k=1}^{n} \left(\frac{\partial q_{tg}^k}{\partial t} \right) \neq 0, \text{ here } R_q = \frac{\frac{\partial q}{\partial t}}{\sum_{k=1}^{n} \left(\frac{\partial q_{tg}^k}{\partial t} \right)} \\ \frac{1}{n} \left(\frac{\partial q_{tg}^k}{\partial t} \right), & \text{if } \sum_{k=1}^{n} \left(\frac{\partial q_{tg}^k}{\partial t} \right) = 0. \end{cases} \tag{43}$$

416

417 **3. Results and discussion**

418 **3.1 Model assessment**

419 Numaguti (1999) pointed out that the results of the tagged AWTs method suffer from the bias of the model used. Therefore,

420 we first estimate the precipitation ~~simulated by the offline version~~in the specified dynamics simulation of CAM5.1, which is

421 compared ~~with~~ to the Global Precipitation Climatology Project (GPCP) version 2.2 combined precipitation data set

422 (Huffman and Bolvin, 2011), as shown in Fig. 2. In winter (December, January and February), high-precipitation zones are

423 located in the tropics of the Southern Hemisphere and in the mid-latitude areas of the NWP. Precipitation is generally less

424 than 3 mm d^{-1} over most parts of Eurasia. In summer (June, July and August), there is heavy precipitation over the southern

425 and southeastern parts of Eurasia and over central Africa. Although CAM5.1 generally shows a bias towards relatively high

426 precipitation in the tropics of the summer hemisphere, the precipitation pattern and amount over Eurasia and its adjacent

427 areas is captured well by CAM5.1. In addition, the water vapour data from the Atmospheric Infrared Sounder (AIRS) and

428 wind fields data from National Centers for Environmental Prediction (NCEP) are~~also~~ used to assess the CAM5.1's results,

429 as shown in Fig. S7. Overall, the water vapour and horizontal wind fields can be well simulated by CAM5.1.

430

431 **3.2 Terrestrial and oceanic contributions to precipitation over Eurasia**

432 Figure 3 shows the spatial distribution of the relative contribution of evaporation from all land source regions to precipitation

433 (colours). In winter, evaporation from land source regions generally contributes ~30–60% to the precipitation over Eurasia.

434 The largest contribution (~80%) is located in central China. In summer, ≥60% of precipitation over most parts of Eurasia is

435   supplied by evaporation from land, especially for the inland region where ≥80% of precipitation originates from the land

436   surface. However, the contribution of evaporation from land to summer precipitation over IND, ICP, and east China is

437   generally less than 50%, due to moisture transport by the Indian summer monsoon and EASM. Overall, the contribution of

438   evaporation from land to precipitation over Eurasia is smaller in winter and larger in summer, which is consistent with the

439   variation of evaporation from the land surface over Eurasia in winter and summer as shown in Fig. 4. The pattern of

440   precipitation contributed by land evaporation is similar to that shown in Numaguti (1999). Our result is close to that of

441   Numaguti (1999) for summer but the contribution of land evaporation to precipitation is evidently larger for winter.

442

443   The distributions of the relative contributions of evaporation from the NAO, the extended north Indian Ocean (includes NIO,

444   BOB, and AS), and the extended Northwest Pacific (includes NWP and SCS), which are three important moisture source

445   regions, are shown in Fig. 5. In winter, ~10–60% of the precipitation over the northern part of Eurasia originates from the

446   NAO, with a westward or northwestward increasing gradient in the relative contribution. The extended north Indian Ocean

447   supplies moisture for ~10–30% of the precipitation over the North Africa and South Asia. The extended Northwest Pacific

448   only provides moisture for 10–30% of the precipitation over the southern and eastern coastal regions of Asia. In summer,

449   evaporation from the NAO only affects precipitation over Europe, with a contribution of 10–30% to total precipitation.

450   Precipitation areas influenced by the extended north Indian Ocean extend to EA, while areas impacted by the extended

451   Northwest Pacific retreat eastward.

452

453   The arrow streamlines in Fig. 3 show the total tropospheric water vapour flux in winter and summer. There is a westward

454   component of water vapour flux over the tropics of both the extended north Indian Ocean and the extended Northwest

455   Pacific in the Northern Hemisphere in winter. In summer, there is a very large northwestward water vapour flux over the

456   NIO, turning northeastward over the BOB and AS. Over the extended Northwest Pacific, there is a northward component of

457   water vapour flux at 30 °–60 °N and a westward flux in the tropics between 120 °E and 180 °E. In addition, Fig. 4 shows strong

458   surface evaporation over the NWP and NAO in winter, while evaporation is weaker in summer. In contrast, evaporation over

459   the NIO is larger in summer and smaller in winter. These results help to explain the variations in the contributions of the

460 NAO, extended north Indian Ocean, and extended Northwest Pacific to precipitation in winter and summer as shown in Fig.

461 5.

462

463 The overall contributions from these three oceanic regions are generally less than those in Numaguti (1999). The resolution

464 of the climate model used in Numaguti (1999) is ~5.6 °, both in latitudinal and longitudinal direction. The different model

465 resolutions are a probable reason for the different quantitative contributions in our study and that of Numaguti (1999). In

466 addition, CAM5.1 is driven by MERRA data, so its surface evaporation flux is approximate to that of MERRA. MERRA

467 land evaporation is larger over South and East Asia and Northern Europe compared to other global estimates (Jiménez et al.,

468 2011), and Bosilovich et al. (2011) suggested that MERRA ocean evaporation is lower compared to other reanalyses but is

469 much closer to observation. Therefore, the bias in MERRA surface evaporation may lead to the higher land contribution and

470 lower oceanic contribution to precipitation.

471

472 **3.3 Atmospheric moisture source attribution of precipitation and water vapour over the YRV**

473 Figures 6a and 6b show the time series of evaporative contribution of each source region to precipitation over the YRV. The

474 contributions of evaporation to precipitation from the BOB and AS are lower during autumn–winter and higher during

475 spring–summer with relative contributions of ≤3.~~6~~9%. Chow et al. (2008) (see their Fig. 20a) also found that evaporation

476 from the AS had little impact on precipitation over China. Supplementary Figs. ~~S7~~S10–S13~~0~~ show the distributions of 25

477 tagged water vapour tracers and 25 tagged precipitations over Eurasia and surrounding areas in winter and summer. Figs.

478 S10~~7~~a and S12~~9~~a show that evaporation from the BOB contributes to water vapour and precipitation over the extended north

479 Indian Ocean in winter, corresponding to the direction of water flux shown in Fig. 3a. The centre of BOB-contributed

480 precipitation (15 mg m^{-2} s^{-1}) is located in the south of the TP in summer (Fig. ~~S10a~~S13a). In addition, the BOB supplies

481 moisture to areas around the northeastern BOB in summer (Fig. ~~S8a~~S11a). The contribution of the SCS to precipitation is

482 also very small (≤~~4.7~~3.4%), which supports the view of Chow et al. (2008), who suggested that the SCS may serve as a

483 pathway for water vapour transport from the southwesterly flow of the Indian summer monsoon and the easterly flow of the

44

484 Northwest Pacific subtropical high. A detailed discussion of this issue is presented in Sect. 3.5. The NWP serves as the

485 dominant oceanic source region for precipitation over the YRV during the whole year except during June and July. The

486 relative contribution is ~~~7.7~~8.1–~~10.1~~10.6% in June and July and ~~14.4~~15.8–~~22.9~~24.6% in other months. As shown in Fig.3,

487 there is strong westward water vapour flux over 20°–45°N for the NWP and southwestward water vapour flux over the

488 tropics of the NWP. ~~But~~However, there is no evident moisture transports from the NWP to EA in the long term mean water

489 vapour flux. Following ~~the~~ Eq. (S1) ~~in the supplement~~, the water vapour flux is divided into the stationary and transient

490 components, as shown in Figs. S8–S9. ~~Figure S8c shows that t~~The transient component of the meridional flux brings some of

491 the moisture from south over most of the NWP and the north of the SCS (Fig. S8c), and ~~Fig. S9c shows that~~ the transient

492 component of the zonal flux leads to westwards water vapour transport over 20°–30°N for the NWP (Fig. S9c). Both the

493 ~~two~~ transient components indicate that the synoptic disturbances can bring moisture originating from the NWP to the

494 southern and eastern coastal regions of Asia during winter. Evaporation from the NIO shows a clear contribution to

495 precipitation during May to October. ~~Especially in June and July~~In particular, the NIO is the dominant oceanic source region

496 in June and July, with a contribution of ~~~22.5~~30%. This is in agreement with the result of a Lagrangian diagnostic method

497 described in Baker et al. (2015) and the result_s of sensitivity experiments in Chow et al. (2008). However, in other months,

498 the contribution of the NIO is very small. The contributions from evaporation from the BOB, AS, and NIO are in phase with

499 the EASM, which was also reported by Baker et al. (2015). The ICP is an important terrestrial source region for the YRV

500 precipitation, supplying moisture to ~9.~~8~~9% of the annual precipitation. The relative contribution of the ICP from April to

501 September is close to the result of Wei et al. (2012). The contribution of evaporation from the YRV to its precipitation can

502 be regarded as the local recycling ratio, which is lower (~~5.9~~4.5–~~9~~7.4%) in summer and higher (~~11~~9.2–~~14.1~~13.4%) in other

503 seasons. In general, the contribution of evaporation from SCN is comparable to the local contribution of the YRV. The

504 relative contribution from the NEA is higher in autumn–winter and lower in spring–summer, which may be associated with

505 the shift of the EA monsoon. Though the individual contributions of evaporation from the YRV or SCN are smaller than

506 those from the NIO in summer, their combined contributions exceed 10%. This implies that evaporation from these two

507 regions is important for precipitation over China. This is contrary to the view expressed in Simmonds et al. (1999) and Qian

508 et al. (2004), but consistent with Wei et al. (2012). Figures 6c and 6d show a time series of evaporative contribution from

509 each source region to the tropospheric water vapour amount over the YRV. The overall relative contribution from each

510 source region to the total water vapour amount is similar to the corresponding relative contribution to precipitation shown in

511 Figs. 6a and 6b.

512

3.4 Atmospheric moisture source attribution of precipitation and water vapour over SCN

514 Figures 7a and 7b show the contribution of each source region to precipitation over SCN. The NIO is the dominant source

515 region in summer, while the NWP dominates precipitation over SCN during other seasons, which is similar to the situation

516 over the YRV. The contribution from the NIO is ~~21.5~~28.4–~~28.1~~37.8% in summer. The contribution from the NWP is 8.~~27~~–

517 ~~15.7~~17.2% in summer and ~~~20~~15.3–~~33.4~~37.2% during other seasons. During spring and summer, ~2.~~2~~4.4% of precipitation

518 is supplied from the BOB, with smaller contributions during other seasons. The contribution from the AS is similar to that of

519 the BOB. In summer, only ~~3~~2.7–~~4.2~~3.7% of precipitation originates from the SCS, but the area contributes ~~~7~~6.7–~~7.3~~7% to

520 the precipitation in early spring (March to April). ~~Like~~ Similar to precipitation over the YRV, the dominant terrestrial source

521 region for SCN is the ICP, which contributes ~~~9.9~~9.8% to the precipitation. In addition, ~~~5.7~~5.6% of summer precipitation

522 originates from SEA. Compared to precipitation over the YRV, the contribution from the TP is smaller. In addition, the

523 contribution from the YRV is small in summer. The local recycling ratio or percentage contribution of evaporation from

524 SCN is generally ~~5.5~~4.3–~~8.8~~7.2% during May to September, but larger than ~~10~~9.3% during the remaining months. As shown

525 in Fig. 7d, the overall relative contribution of each source region to the water vapour amount is similar to each region's

526 contribution to precipitation over SCN.

527

3.5 Atmospheric moisture source attribution of water vapour over the SCS

529 Simmonds et al. (1999) and Lau et al. (2002) suggested that interannual variation of summer precipitation over China is

530 associated with water vapour transport over the SCS. However, Chow et al. (2008) suggested that the SCS may act as a

531 water vapour transport pathway where the southwesterly stream of the Indian summer monsoon and the easterly stream of

the southeastern Asian monsoon meet. Previous studies have conducted sensitivity experiments or analysed the water vapour budget to indirectly determine moisture sources for the SCS. In contrast, our AWT method can directly quantify the contribution of each source region to the water vapour amount over the SCS, which is shown in Fig. 8. The local contribution of the SCS is small (~~~5~~4.7 ~~5.8~~5.5%) in summer, and the mean contribution in other months is ~~~7.4~~6.8%. The contribution of the NIO shows clear seasonal variations: the contribution is high during May to October, but very small during the other months. Similar to the results for water vapour over the YRV and SCN, the NIO is the dominant source region from June to September, with a contribution of ~~20.8~~22.7 ~~26.9~~31%. During this period, the contribution of the NWP is ~~13.3~~14.1 ~~19~~21.2%. However, the NWP dominates the water vapour over the SCS in the remaining months, with contributions of ~~23.8~~25.7 ~~45.1~~51.3%. In addition, the SP and NEP are also important oceanic source regions, with combined annual contributions of ~~~13~~11 ~~17.7~~16.6%. The most important terrestrial moisture source region is the SEA, whose contribution is larger (13.~~7~~8–16.~~1~~2%) in summer and smaller (~~~6.4~~5.3%) in winter. During late autumn to winter, about 5.~~2~~3–6.~~2~~3% of water vapour is supplied from NEA, but its contribution is very small in other seasons. The other land source regions contribute relatively little to the water vapour amount over the SCS.

From the SCS to SCN and further to the YRV (from south to north), surface evaporation from the SCS generally represents a small (≤5.~~8~~5%) contribution to the water vapour amount over the three target areas in summer. In contrast, much more water vapour is supplied by evaporation from the NWP and NIO. This confirms the inference proposed by Chow et al. (2008) that the SCS is a water vapour transport pathway where moisture from the NIO and NWP meet in summer.

4. Conclusions

In this study, an Eulerian tagged AWT method was implemented in CAM5.1, which provides the capacity to separately trace the behaviour of atmospheric water substances originating from various moisture source regions and to quantify their contributions to atmospheric water over an arbitrary region. Numaguti (1999) pointed out that the weakness of the tagged AWT method is that its results suffer from the performance of the model in reproducing the hydrological cycle. However, a

comparison between GPCP and CAM5.1 precipitation shows that CAM5.1 has the capability to represent total precipitation ~~processes~~. CAM5.1 also can reproduce water vapour and large scale circulation reasonable, as compared to AIRS and NCEP data. Using this method, we investigated the contribution of evaporation from land, as well as the contributions from the North Atlantic Ocean~~NAO~~, extended north Indian Ocean, and extended Northwest Pacific to precipitation over Eurasia. Our results are similar to those of Numaguti (1999), except that our results indicate a larger contribution from terrestrial source regions, while the three oceanic regions show smaller contributions. Different model resolutions and a bias in MERRA surface evaporation are probable causes for the differences between our results and those of Numaguti (1999).

We then investigated the contribution of various source regions to precipitation and water vapour amounts over the YRV and SCN. Our results suggest that the dominant oceanic moisture source region during summer is the NIO (~~15.9~~20.5–~~22.5~~30.3% of precipitation over the YRV; ~~21.5~~28.4–~~28.1~~37.8% of precipitation over SCN), consistent with Baker et al. (2015) and Chow et al. (2008), while during other seasons, the NWP is the dominant source region (~~14.3~~15.8–~~22.9~~24.6% of precipitation over the YRV; ~~14.4~~15.3–~~34.1~~37.1% of precipitation over SCN), with smaller contributions from the BOB, AS, and SCS. The ICP is an important terrestrial source region, with a mean annual contribution of ~10%. For precipitation over the YRV, the combined contribution of evaporation from the YRV and SCN is non-negligible (exceeding 10%), consistent with Wei et al. (2012). For precipitation over SCN, the local recycling ratio is generally ~~5.5~~4.3–~~8.8~~7.2% during May to September, and reaches ~~11.1~~9.4–~~19.6~~18.7% in other months. The contribution from the YRV is very small in summer. The overall relative contribution of each source region to the water vapour amount is similar to the corresponding contribution to precipitation over the YRV and SCN.

An analysis of water vapour amount over the SCS shows that the NIO is the dominant source region (~~20.8~~22.7–~~26.9~~31% of water vapour) during June to September, while the NWP dominates (~~23.8~~25.7–~~45.1~~51.3% of water vapour) in the remaining months. In contrast, the local contribution of the SCS is smaller (~~~5~~4.7–~~5.8~~5.5%) in summer. In addition, the SP, NEP, and SEA are also important source regions. Evaporation over the SCS represents a small contribution to water vapour amounts

580 over the SCS, SCN, and the YRV in summer, implying that the SCS acts as a water vapour transport pathway rather than a

581 dominant source region, which confirms the inference of Chow et al. (2008).

582

583 At present, the tagged AWT method has only been applied to a few GCMs and regional models, and has generally focused

584 on identifying the moisture distribution over a few regions such as NAM North America (Bosilovich and Schubert, 2002;

585 Bosilovich et al., 2003). We expect that the AWT method will be applied to additional models and used to identify moisture

586 sources over more climate regions, which will improve our understanding of atmospheric moisture transport.

587

Code availability

589 The source code modifications for CAM5.1 are available from the authors. Interested readers should contact us via

590 arthur_pc@163.com or binzhu@nuist.edu.cn.

591

596

References

598 Baker, A. J., Sodemann, H., Baldini, J. U. L., Breitenbach, S. F. M., Johnson, K. R., van Hunen, J., and Zhang, P.:

599   Seasonality of westerly moisture transport in the East Asian summer monsoon and its implications for interpreting

600   precipitation δ^{18}O, J. Geophys. Res. Atmos., 120(12), 5850–5862, doi:10.1002/2014JD022919, 2015.

49

601 Bosilovich, M. G.: On the vertical distribution of local and remote sources of water for precipitation, Meteorol. Atmos. Phys.,

602   80(1), 31–41, doi:10.1007/s007030200012, 2002.

603 Bosilovich, M. G. and Schubert, S. D.: Water vapor tracers as diagnostics of the regional hydrologic cycle, J.

604   Hydrometeorol., 3(2), 149–165, doi:http://dx.doi.org/10.1175/1525-7541(2002)003<0149:WVTADO>2.0.CO;2, 2002.

605 Bosilovich, M. G., Robertson, F. R., Chen, J.: Global energy and water budgets in MERRA, J. Climate, 24(22), 5721–5739,

606   doi:http://dx.doi.org/10.1175/2011JCLI4175.1, 2011.

607 Bosilovich, M. G., Sud, Y. C., Schubert, S. D., and Walker, G. K.: Numerical simulation of the large-scale North American

608   monsoon water sources, J. Geophys. Res. Atmos., 108(D16), 8614, doi:10.1029/2002JD003095, 2003.

609 Bretherton, C. S., McCaa, J. R., and Grenier, H.: A new parameterization for shallow cumulus convection and its application

610   to marine subtropical cloud-topped boundary layers. Part I: Description and 1D results, Mon. Wea. Rev., 132(4), 864–

611   882, doi:http://dx.doi.org/10.1175/1520-0493(2004)132<0883:ANPFSC>2.0.CO;2, 2004.

612 Bretherton, C. S. and Park, S.: A new moist turbulence parameterization in the Community Atmosphere Model, J. Climate,

613   22(12), 3422–3448, doi:http://dx.doi.org/10.1175/2008JCLI2556.1, 2009.

614 Brubaker, K. L., Entekhabi, D., and Eagleson, P. S.: Estimation of continental precipitation recycling, J. Clim., 6(6), 1077–

615   1089, doi:http://dx.doi.org/10.1175/1520-0442(1993)006<1077:EOCPR>2.0.CO;2, 1993.

616 Burde, G. I. and Zangvil, A.: The estimation of regional precipitation recycling. Part I: Review of recycling models, J. Clim.,

617   14(12), 2497–2508, doi:http://dx.doi.org/10.1175/1520-0442(2001)014<2497:TEORPR>2.0.CO;2, 2001.

618 Chen, B., Xu, X. D., and Zhao, T.: Main moisture sources affecting lower Yangtze River Basin in boreal summers during

619   2004–2009, Int. J. Climatol., 33(4), 1035–1046, doi:10.1002/joc.3495, 2013.

620 Chow, K. C., Tong, H. W., and Chan, J. C.: Water vapor sources associated with the early summer precipitation over China,

621   Clim. Dynam., 30(5), 497–517, doi:10.1007/s00382-007-0301-6, 2008.

622 Dirmeyer, P. A. and Brubaker, K. L.: Contrasting evaporative moisture sources during the drought of 1988 and the flood of

623   1993, J. Geophys. Res., 104(D16), 19383–19397, doi:10.1029/1999JD900222, 1999.

624 Drumond, A., Nieto, R., and Gimeno, L.: Sources of moisture for China and their variations during drier and wetter

625   conditions in 2000−2004: a Lagrangian approach, Clim. Res., 5, 215–225, doi:10.3354/cr01043, 2011.

Eltahir, E. A. and Bras, R. L.: Precipitation recycling, Rev. Geophys., 34(3), 367–378, doi:10.1029/96RG01927, 1996.

Emmons, L. K., Walters, S., Hess, P. G., Lamarque, J.-F., Pfister, G. G., Fillmore, D., Granier, C., Guenther, A., Kinnison, D., Laepple, T., Orlando, J., Tie, X., Tyndall, G., Wiedinmyer, C., Baughcum, S. L., and Kloster, S.: Description and evaluation of the Model for Ozone and Related chemical Tracers, version 4 (MOZART-4), Geosci. Model Dev., 3(1), 43–67, doi:10.5194/gmd-3-43-2010, 2010.

Gettelman, A., Liu, X., Ghan, S. J., Morrison, H., Park, S., Conley, A. J., Klein, S. A., Boyle, J., Mitchell, D. L., and Li, J.-L. F.: Global simulations of ice nucleation and ice supersaturation with an improved cloud scheme in the Community Atmosphere Model, J. Geophys. Res., 115, D18216, doi:10.1029/2009JD013797, 2010.

Gimeno, L., Stohl, A., Trigo, R. M., Dominguez, F., Yoshimura, K., Yu, L., Drumond, A., Durán-Quesada, A. M., and Nieto, R.: Oceanic and terrestrial sources of continental precipitation, Rev. Geophys., 50, RG4003, doi:10.1029/2012RG000389, 2012.

Gustafsson, M., Rayner, D. and Chen, D.: Extreme rainfall events in southern Sweden: where does the moisture come from? Tellus A, 62, 605–616, doi:10.1111/j.1600-0870.2010.00456.x, 2010.

Held, I. M. and Soden, B. J.: Water vapor feedback and global warming, Annu. Rev. Energy Environ., 25, 441–475, doi:10.1146/annurev.energy.25.1.441, 2000.

Horowitz, L. W., Walters, S., Mauzerall, D. L., Emmons, L. K., Rasch, P. J., Granier, C., Tie, X. X., Lamarque, J.-F., Schultz, M. G., Tyndall, G. S., Orlando, J. J., and Brasseur, G. P.: A global simulation of tropospheric ozone and related tracers: Description and evaluation of MOZART, version 2, J. Geophys. Res., 108, 4784, doi:10.1029/2002JD002853, 2003.

Huffman, G. J. and Bolvin, D. T.: GPCP version 2.2 combined precipitation data set documentation, NASA Goddard Space Flight Center, Mesoscale Atmospheric Processes Laboratory and Science Systems and Applications, Inc., 2011.

Jiménez, C., Prigent, C., Mueller, B., Seneviratne, S. I., McCabe, M. F., Wood, E. F., Rossow, W. B., Balsamo, G., Betts, A. K., Dirmeyer, P. A., Fisher, J. B., Jung, M., Kanamitsu, M., Reichle, R. H., Reichstein, M., Rodell, M., Sheffield, J., Tu, K., and Wang, K.: Global intercomparison of 12 land surface heat flux estimates, J. Geophys. Res., 116, D02102, doi:10.1029/2010JD014545, 2011.

651 Joussaume, S., Sadourny, R., and Vignal, C.: Origin of precipitating water in a numerical simulation of the July climate,
652   Ocean-Air Inter., 1, 43–56, 1986.

653 Knoche, H. R. and Kunstmann, H.: Tracking atmospheric water pathways by direct evaporation tagging: A case study for
654   West Africa, J. Geophys. Res. Atmos., 118, 12345–12358, doi:10.1002/2013JD019976, 2013.

655 Koster, R., Jouzel, J., Suozzo, R., Russell, G., Broecker, W., Rind, D., and Eagleson, P.: Global sources of local precipitation
656   as determined by the NASA/GISS GCM, Geophys. Res. Lett., 13(2), 121–124, doi:10.1029/GL013i002p00121, 1986.

657 Lamarque, J.-F., Emmons, L. K., Hess, P. G., Kinnison, D. E., Tilmes, S., Vitt, F., Heald, C. L., Holland, E. A., Lauritzen, P.
658   H., Neu, J., Orlando, J. J., Rasch, P. J., and Tyndall, G. K.: CAM-chem: description and evaluation of interactive
659   atmospheric chemistry in the Community Earth System Model, Geosci. Model Dev., 5, 369–411, doi:10.5194/gmd-5-
660   369-2012, 2012.

661 Lau, K. M., Li, X., and Wu, H. T.: Evolution of the large scale circulation, cloud structure and regional water cycle
662   associated with the South China Sea monsoon during May–June, 1998, J. Meteor. Soc. Japan. Ser. II, 80(5), 1129–1147,
663   doi:10.2151/jmsj.80.1129, 2002.

664 Lin, Y. L., Farley, R. D., and Orville, H. D.: Bulk parameterization of the snow field in a cloud model, J. Climate Appl.
665   Meteor., 22(6), 1065–1092, doi:http://dx.doi.org/10.1175/1520-0450(1983)022<1065:BPOTSF>2.0.CO;2, 1983.

666 Morrison, H. and Gettelman, A.: A new two-moment bulk stratiform cloud microphysics scheme in the Community
667   Atmosphere Model, version 3 (CAM3). Part I: Description and numerical tests, J. Climate, 21(15), 3642–3659,
668   doi:http://dx.doi.org/10.1175/2008JCLI2105.1, 2008.

669 Morrison, H. and Pinto, J. O.: Mesoscale modeling of springtime Arctic mixed-phase stratiform clouds using a new two-
670   moment bulk microphysics scheme, J. Atmos. Sci., 62(10), 3683–3704, doi:http://dx.doi.org/10.1175/JAS3564.1, 2005.

671 Neale, R. B., Chen, C.-C., Gettelman, A., Lauritzen, P. H., Park, S., Williamson, D. L., Conley, A. J., Garcia, R., Kinnison,
672   D., Lamarque, J.-F., Marsh, D., Mills, M., Smith, A. K., Tilmes, S., Vitt, F., Morrison, H., Gameron-Smith, P., Collins,
673   W. D., Iacono, M. J., Easter, R. C., Ghan, S. J., Liu, X., Rasch, P. J., and Taylor, M. A.: Description of the NCAR
674   Community Atmosphere Model (CAM5), NCAR Technical Note NCAR/TN-486+STR, 275 pp, 2012.

675 Numaguti, A.: Origin and recycling processes of precipitating water over the Eurasian continent: Experiments using an

676   atmospheric general circulation model, J. Geophys. Res., 104(D2), 1957–1972, doi:10.1029/1998JD200026, 1999.

677 Park, S. and Bretherton, C. S.: The University of Washington shallow convection and moist turbulence schemes and their

678   impact on climate simulations with the Community Atmosphere Model, J. Climate, 22(12), 3449–3469,

679   doi:http://dx.doi.org/10.1175/2008JCLI2557.1, 2009.

680 Park, S., Bretherton, C. S., and Rasch, P. J.: Integrating cloud processes in the Community Atmosphere Model, version 5, J.

681   Climate, 27(18), 6821–6856, doi:http://dx.doi.org/10.1175/JCLI-D-14-00087.1, 2014.

682 Qian, J. H., Tao, W. K., and Lau, K. M.: Mechanisms for Torrential Rain Associated with the Mei-Yu Development during

683   SCSMEX   1998,   Mon.   Wea.   Rev.,   132(1),   3–27,   doi:http://dx.doi.org/10.1175/1520-

684   0493(2004)132<0003:MFTRAW>2.0.CO;2, 2004.

685 Rasch, P. J., Coleman, D. B., Mahowald, N., and Williamson, D. L.: Characteristics of Atmospheric Transport Using Three

686   Numerical Formulations for Atmospheric Dynamics in a Single GCM Framework, J. Climate, 19(11), 2243–2266,

687   doi:http://dx.doi.org/10.1175/JCLI3763.1, 2006.

688 Rasch, P. J., Mahowald, N. M., and Eaton, B. E.: Representations of transport, convection, and the hydrologic cycle in

689   chemical transport models: Implications for the modeling of short-lived and soluble species, J. Geophys. Res., 102,

690   28127–28138, doi:10.1029/97JD02087, 1997.

691 Raymond, D. J. and Blyth, A. M.: A stochastic mixing model for nonprecipitating cumulus clouds, J. Atmos. Sci., 43(22),

692   2708–2718, doi:http://dx.doi.org/10.1175/1520-0469(1986)043<2708:ASMMFN>2.0.CO;2, 1986.

693 Raymond, D. J. and Blyth, A. M.: Extension of the stochastic mixing model to cumulonimbus clouds, J. Atmos. Sci., 49(21),

694   1968–1983, doi:http://dx.doi.org/10.1175/1520-0469(1992)049<1968:EOTSMM>2.0.CO;2, 1992.

695 Reisner, J., Rasmussen, R. M., and Bruintjes, R. T.: Explicit forecasting of supercooled liquid water in winter storms using

696   the MM5 mesoscale model, Quart. J. Roy. Meteor. Soc., 124(548), 1071–1107, doi:10.1002/qj.49712454804, 1998.

697 Richter, J. H. and Rasch, P. J.: Effects of convective momentum transport on the atmospheric circulation in the community

698   atmosphere model, version 3, J. Climate, 21(7), 1487–1499, doi:http://dx.doi.org/10.1175/2007JCLI1789.1, 2008.

699 Rienecker, M. M., Suarez, M. J., Gelaro, R., Todling, R., Bacmeister, J., Liu, E., Bosilovich, M. G., Schubert, S. D., Takacs,

700 L., Kim, G.-K., Bloom, S., Chen, J., Collins, D., Conaty, A., da Silva, A., Gu, W., Joiner, J., Koster, R. D., Lucchesi, R.,

701 Molod, A., Owens, T., Pawson, S., Pegion, P., Redder, C. R., Reichle, R., Robertson, F. R., Ruddick, A. G.,

702 Sienkiewicz, M., and Woollen, J.: MERRA: NASA's Modern-Era Retrospective analysis for Research and Applications,

703 J. Climate, 24(14), 3624–3648, doi:http://dx.doi.org/10.1175/JCLI-D-11-00015.1, 2011.

704 Savenije, H. H. G.: New definitions for moisture recycling and the relationship with land-use changes in the Sahel, J. Hydrol.,

705 167, 57–78, doi:10.1016/0022-1694(94)02632-L, 1995.

706 Simmonds, I., Bi, D. and Hope, P.: Atmospheric Water Vapor Flux and Its Association with Rainfall over China in Summer,

707 J. Climate, 12(5), 1353–1367, doi:http://dx.doi.org/10.1175/1520-0442(1999)012<1353:AWVFAI>2.0.CO;2, 1999.

708 Sodemann, H. and Zubler, E.: Seasonal and interannual variability of the moisture sources for Alpine precipitation during

709 1995–2002, Int. J. Climatol., 30, 947–961, doi:10.1002/joc.1932, 2010.

710 Sodemann, H., Schwierz, C., and Wernli, H.: Interannual variability of Greenland winter precipitation sources: Lagrangian

711 moisture diagnostic and North Atlantic Oscillation influence, J. Geophys. Res., 113, D03107,

712 doi:10.1029/2007JD008503, 2008.

713 Sodemann, H., Wernli, H. and Schwierz, C.: Sources of water vapour contributing to the Elbe flood in August 2002—A

714 tagging study in a mesoscale model, Q.J.R. Meteorol. Soc., 135, 205–223, doi:10.1002/qj.374, 2009.

715 Stohl, A. and James, P.: A Lagrangian analysis of the atmospheric branch of the global water cycle. Part I: Method

716 description, validation, and demonstration for the August 2002 flooding in central Europe, J. Hydrometeor., 5(4),

717 656–678, doi:http://dx.doi.org/10.1175/1525-7541(2004)005<0656:ALAOTA>2.0.CO;2, 2004.

718 Stohl, A., Forster, C., and Sodemann, H.: Remote sources of water vapor forming precipitation on the Norwegian west coast

719 at 60 °N – a tale of hurricanes and an atmospheric river, J. Geophys. Res., 113, D05102, doi:10.1029/2007JD009006,

720 2008.

721 Sundqvist, H.: Parameterization of condensation and associated clouds in models for weather prediction and general

722 circulation simulation, Physically-based modelling and simulation of climate and climatic change, Springer Netherlands,

723 pp 433–461, 1998.

724 Thompson, G., Rasmussen, R. M., and Manning, K.: Explicit forecasts of winter precipitation using an improved bulk

725   microphysics scheme. Part I: Description and sensitivity analysis, Mon. Wea. Rev., 132(2), 519–542,

726   doi:http://dx.doi.org/10.1175/1520-0493(2004)132<0519:EFOWPU>2.0.CO;2, 2004

727 Trenberth, K. E.: Atmospheric moisture recycling: Role of advection and local evaporation, J. Clim., 12(5), 1368–1381,

728   doi:http://dx.doi.org/10.1175/1520-0442(1999)012<1368:AMRROA>2.0.CO;2, 1999.

729 Wei, J., Dirmeyer, P. A., Bosilovich, M. G., and Wu, R.: Water vapor sources for Yangtze River Valley rainfall:

730   Climatology, variability, and implications for rainfall forecasting, J. Geophys. Res. Atmos., 117, D05126,

731   doi:10.1029/2011JD016902, 2012.

732 Xu, X. D., Shi, X. Y., Wang, Y. Q., Peng, S. Q., and Shi, X. H.: Data analysis and numerical simulation of moisture source

733   and transport associated with summer precipitation in the Yangtze River Valley over China, Meteorol. Atmos. Phys.,

734   100(1), 217–231, doi:10.1007/s00703-008-0305-8, 2008.

735 Zhang, G. J. and McFarlane, N. A.: Sensitivity of climate simulations to the parameterization of cumulus convection in the

736   Canadian   Climate   Centre   general   circulation   model,   Atmos.   Ocean,   33(3),   407–446,

737   doi:10.1080/07055900.1995.9649539, 1995.

738 Zhang, M., Lin, W., Bretherton, C., Hack, J., and Rasch, P. J.: A modified formulation of fractional stratiform condensation

739   rate   in   the   NCAR   Community   Atmospheric   Model   (CAM2), J.   Geophys.   Res., 108(D1),   4035,

740   doi:10.1029/2002JD002523, 2003.

741
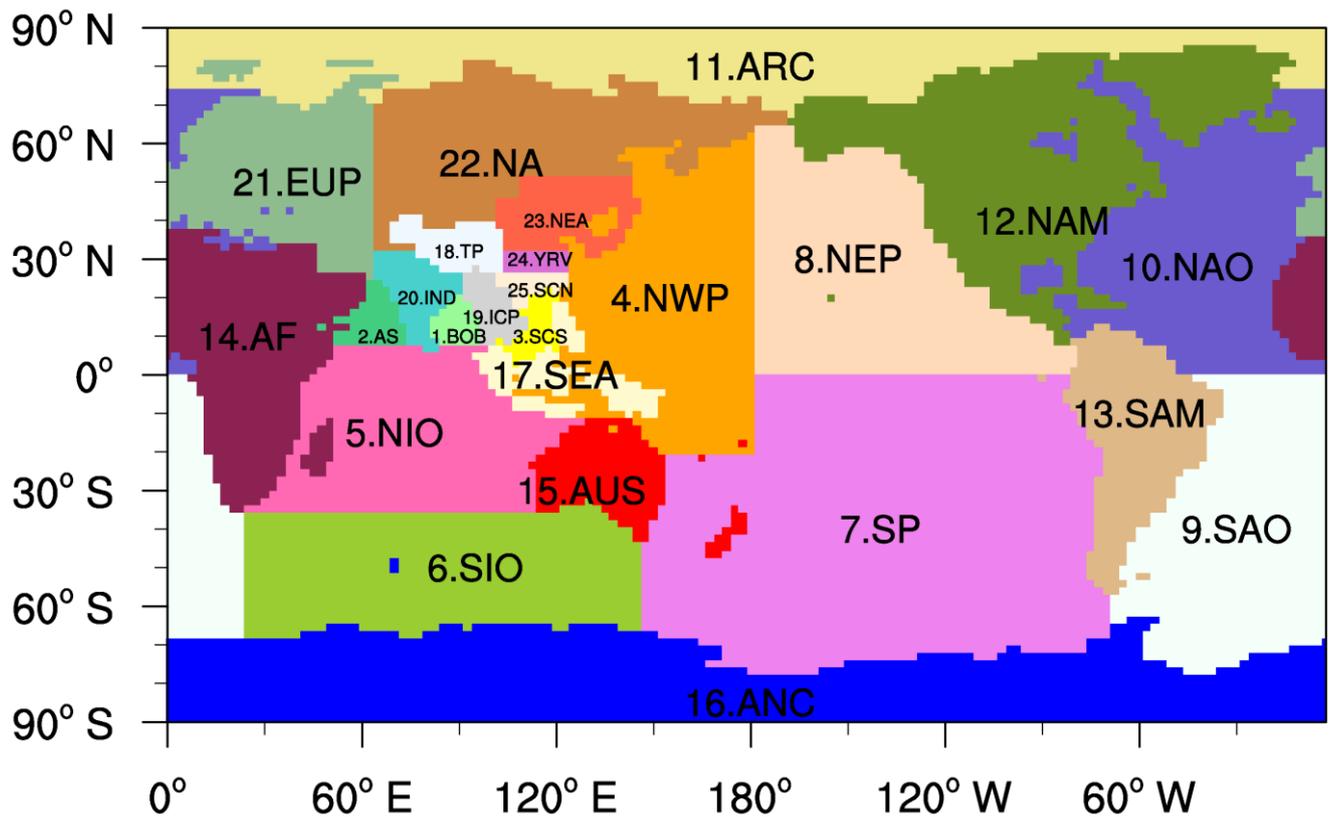
Figure 1. Moisture source regions: the regions are denoted as (1) Bay of Bengal: BOB; (2) Arabian Sea: AS; (3) South China Sea: SCS; (4) Northwest Pacific: NWP; (5) north Indian Ocean: NIO; (6) southern Indian Ocean: SIO; (7) southern Pacific: SP; (8) Northeast Pacific: NEP; (9) southern Atlantic Ocean: SAO; (10) northern Atlantic Ocean: NAO; (11) Arctic Ocean: ARC; (12) North America: NAM; (13) South America: SAM; (14) Africa: AF; (15) Australia: AUS; (16) Antarctic: ANC; (17) Southeast Asia: SEA; (18) Tibet Plateau: TP; (19) Indo-China Peninsula: ICP; (20) India: IND; (21) Europe: EUP; (22) North Asia: NA; (23) Northeast Asia: NEA; (24) Yangtze River Valley: YRV; (25) South China: SCN.

749
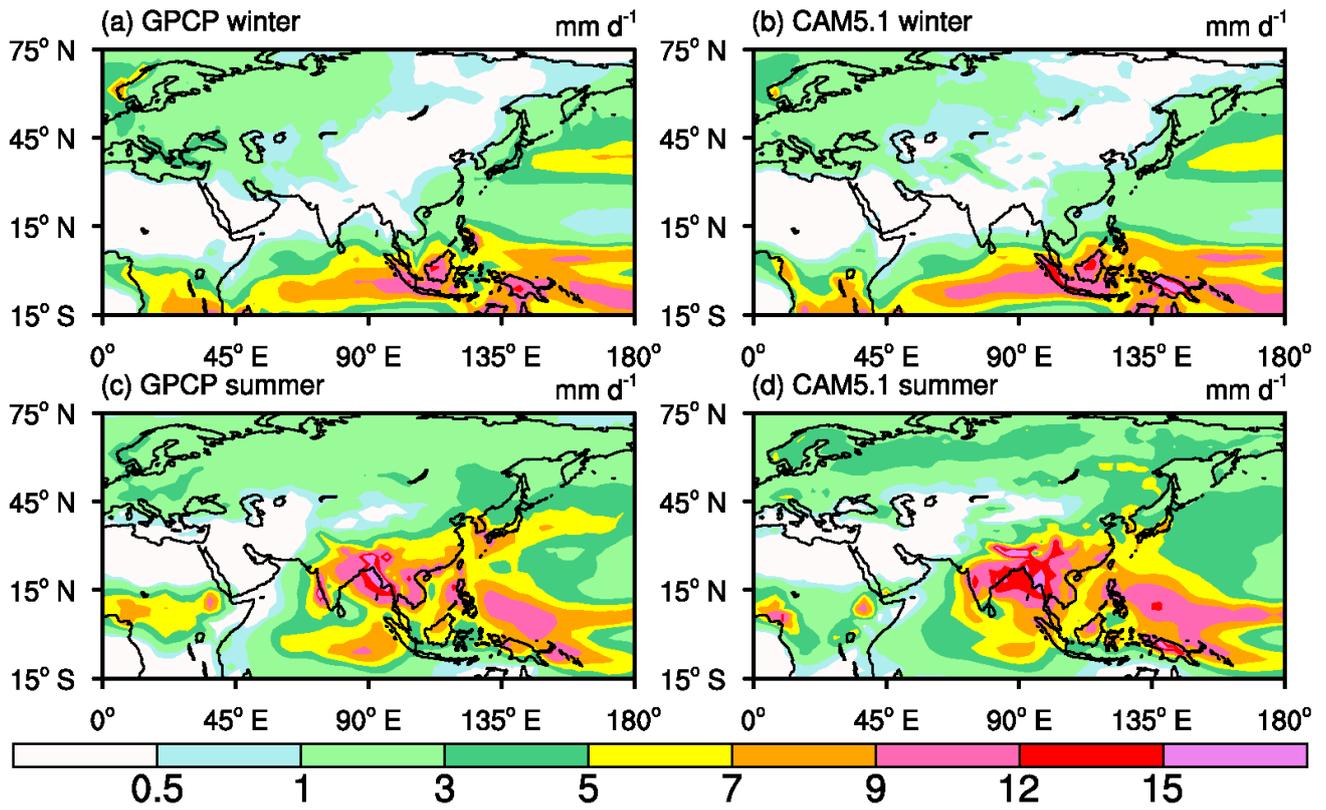
Figure 2. Comparisons between (left) GPCP data and (right) CAM5.1 precipitation simulations during (top) winter and (bottom) summer

751 (ten-year averages for 1998 to 2007).
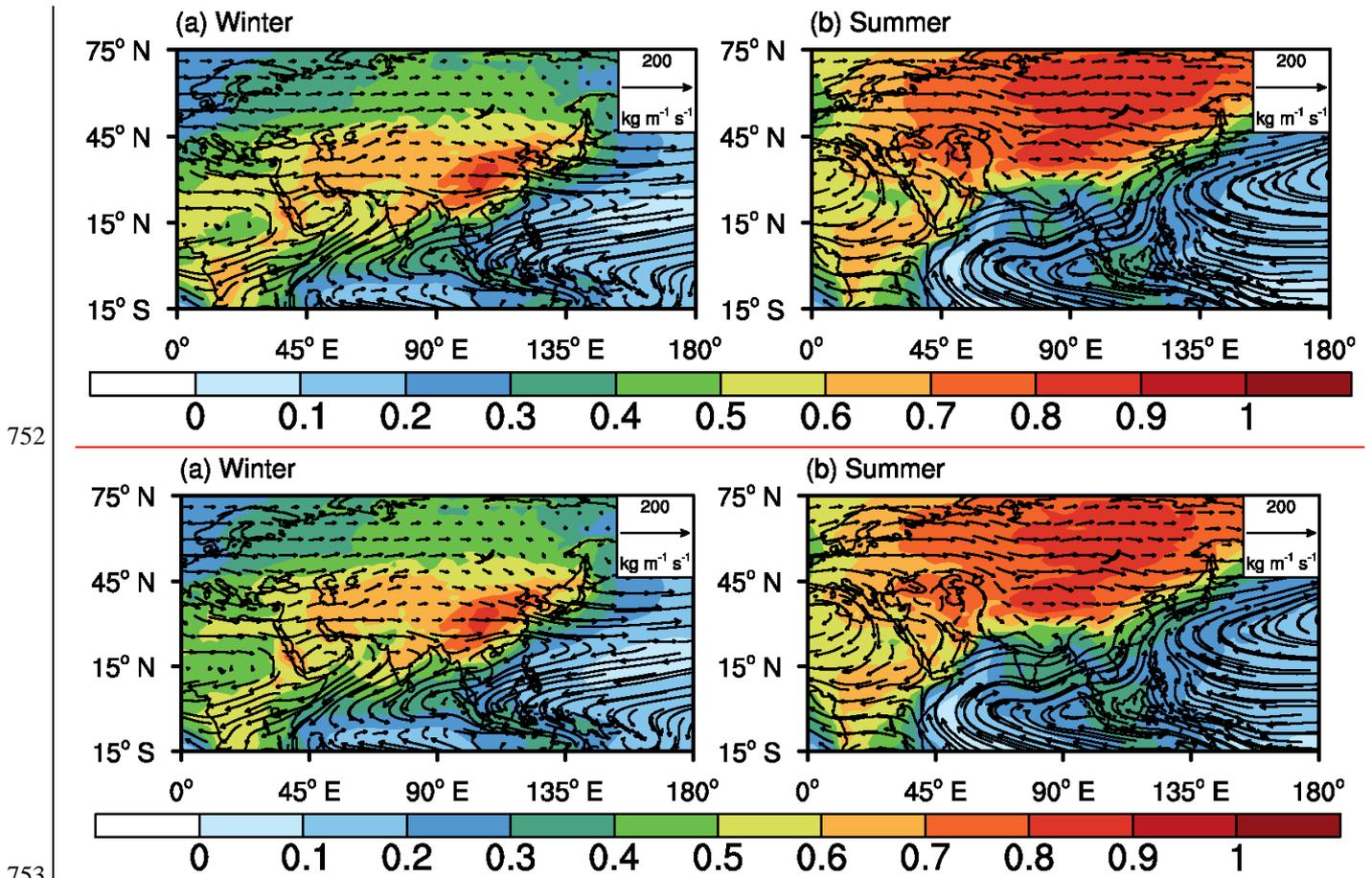
Figure 3. Distribution of the relative contribution to precipitation from all land source regions defined in **Fig. 1** (colours, unit: 1 ratio of tagged precipitation over total precipitation) and the vertically integrated total tropospheric water vapour flux (arrow streamlines, unit: kg m^{-1} s^{-1}) during (a) winter and (b) summer.
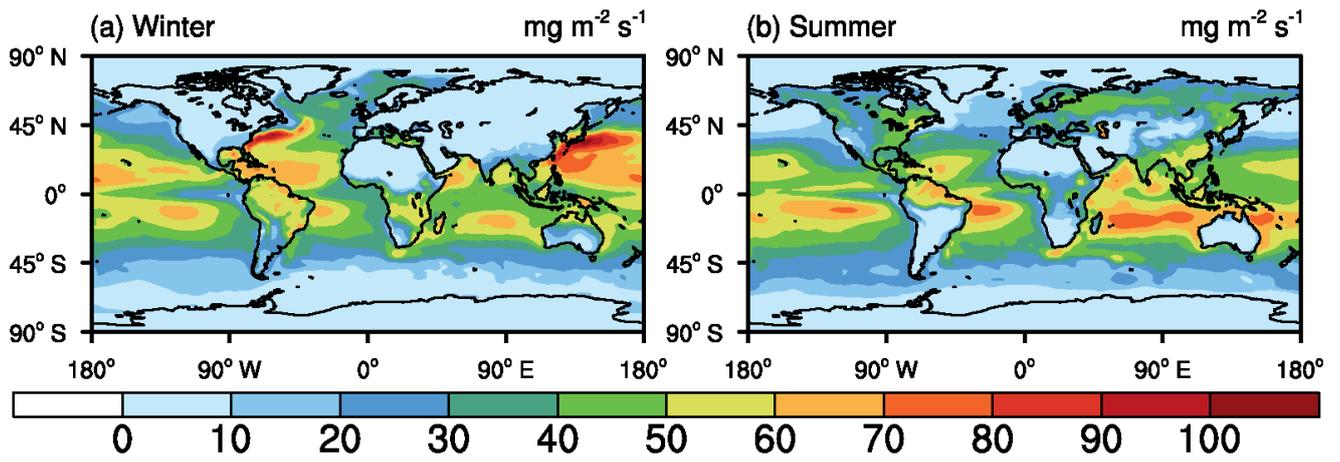
Figure 4. Distribution of CAM5.1's ten-year averaged surface evaporation flux (unit: mg m^{-2} s^{-1}) in (a) winter and (b) summer between 1998 and 2007.
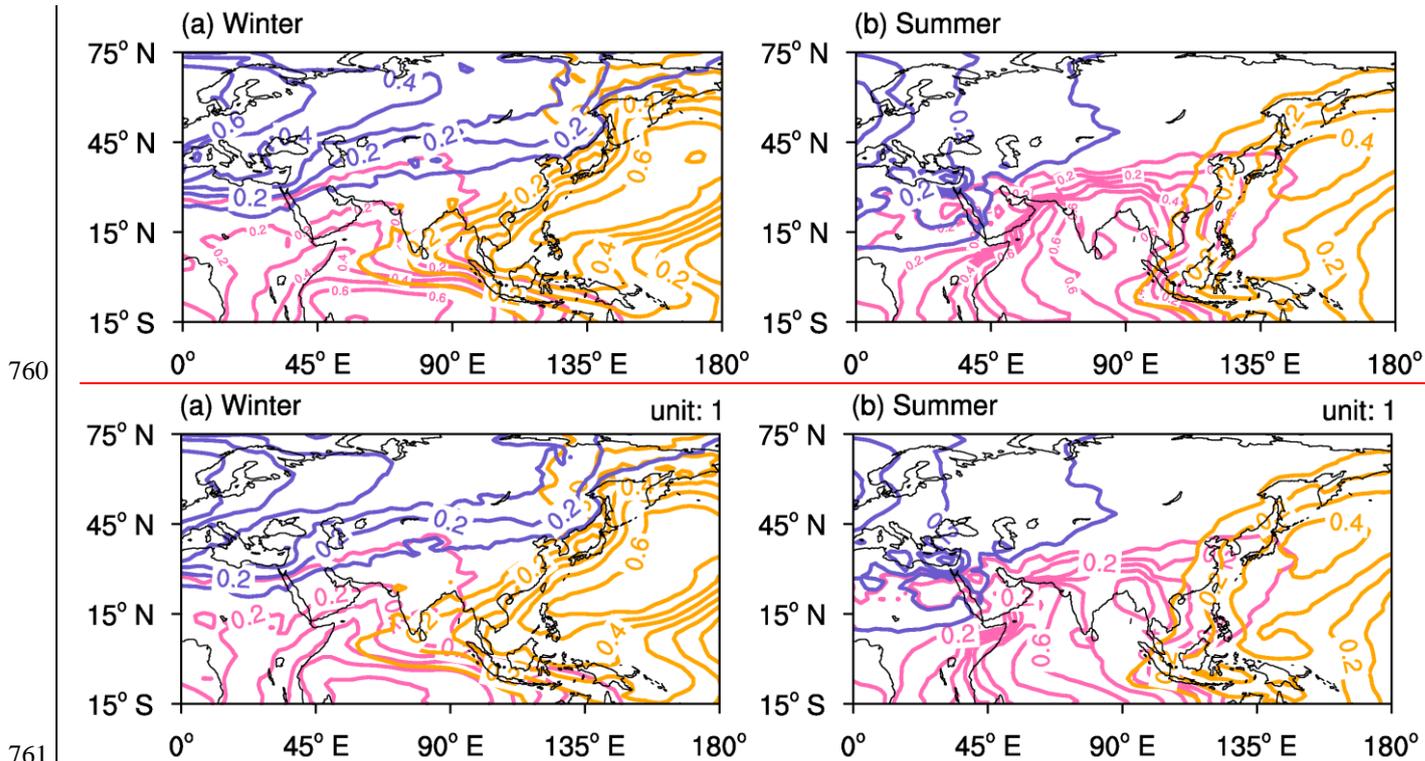
Figure 5. Distributions of the ratios of precipitation (unit: ~~1~~ratio of tagged precipitation over total precipitation) supplied from the NAO (slate blue), the extended north Indian Ocean (NIO + BOB + AS, pink), and the extended Northwest Pacific (NWP + SCS, orange) during (a) winter and (b) summer. Contour interval is 0.1.
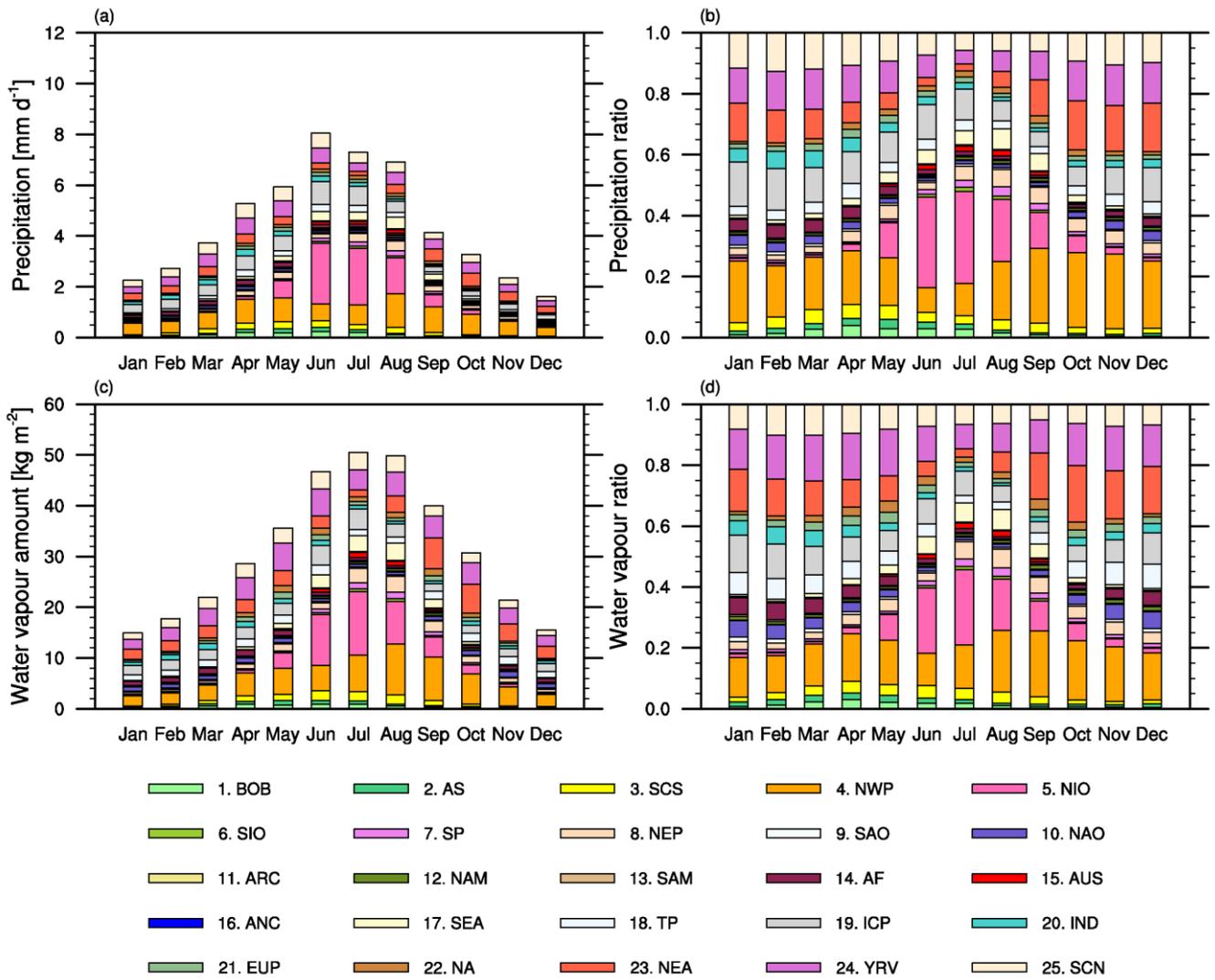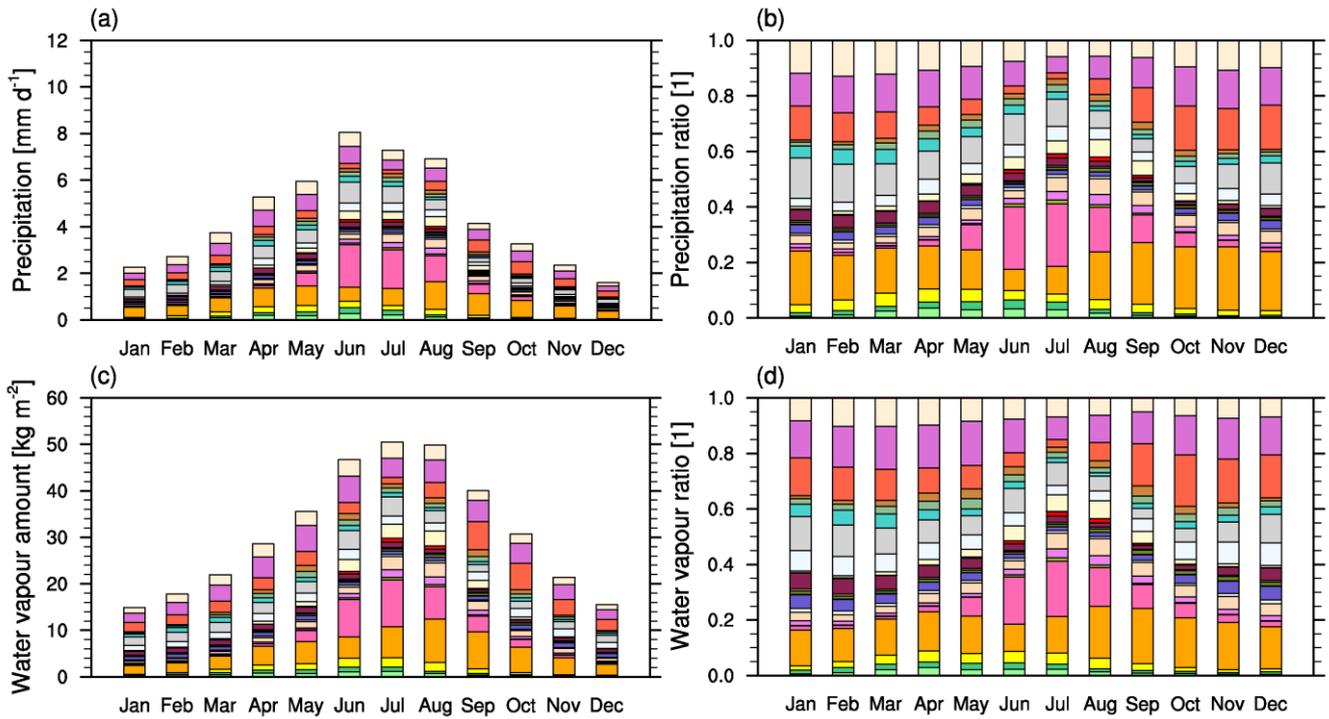
Figure 6. (a) Monthly averaged evaporative contributions of 25 defined source regions to the precipitation over the YRV. (b) Same as **Fig. 6a**, but for the relative contribution to precipitation. (c) Monthly averaged evaporative contributions of 25 defined source regions to the tropospheric total water vapour amount over the YRV. (d) Same as **Fig. 6c**, but for the relative contribution to water vapour. Stacked column colours correspond to source region colours in **Fig. 1**.
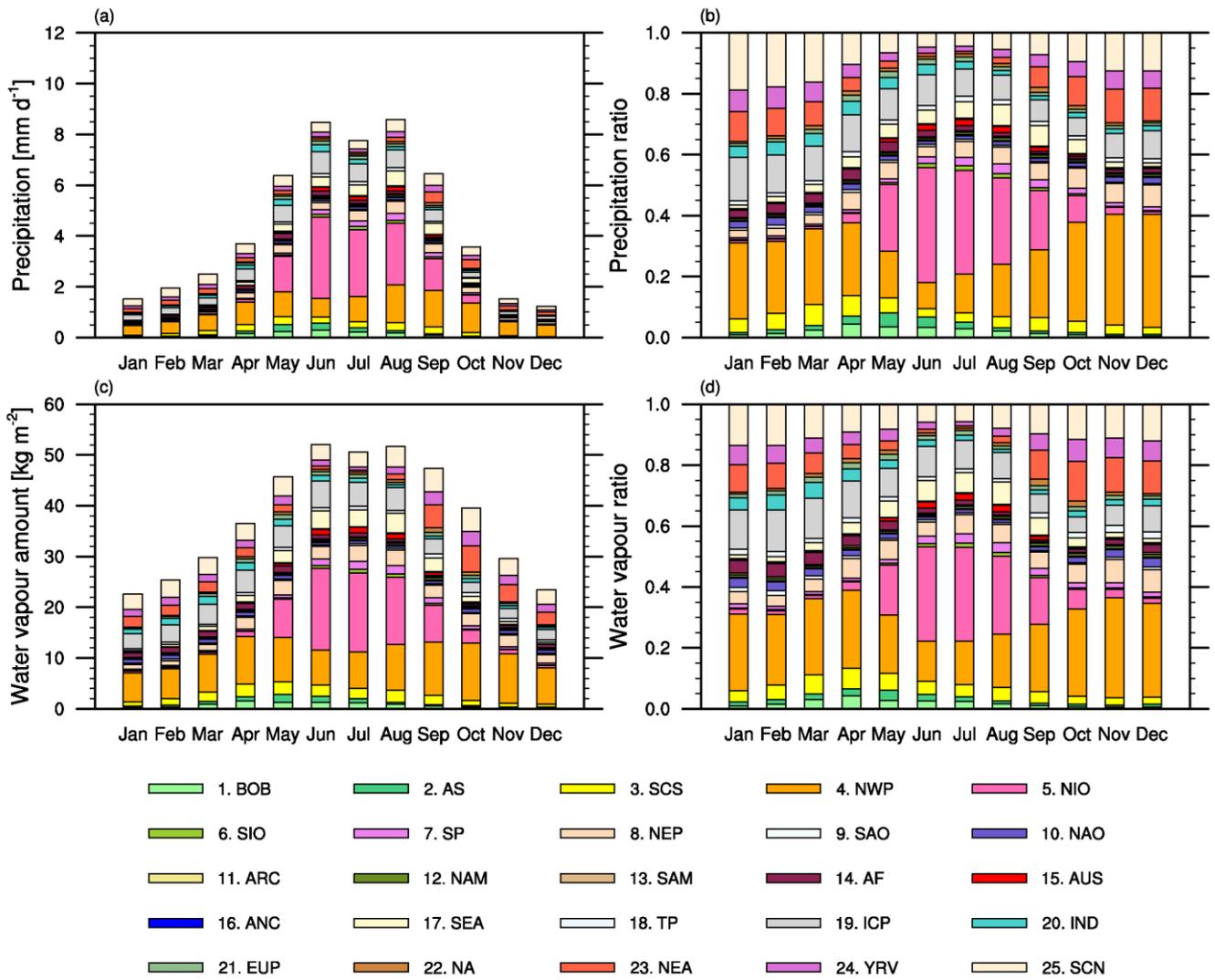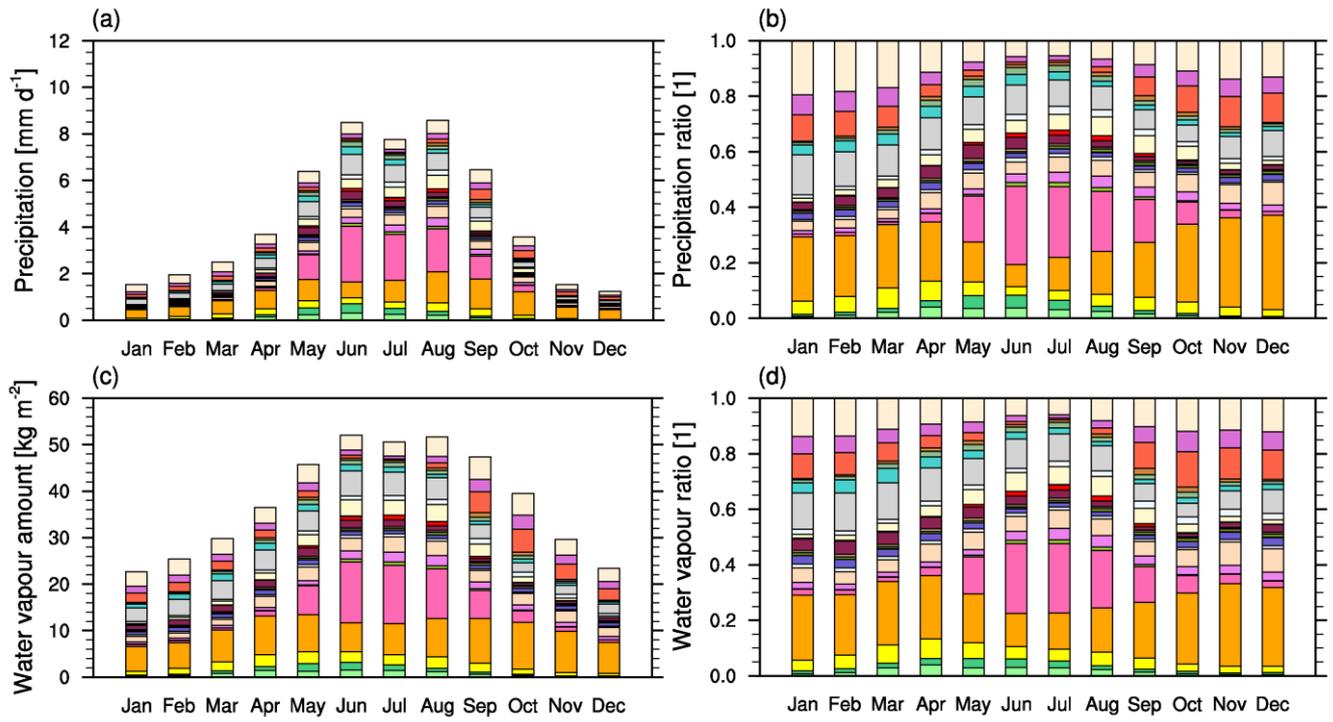
Figure 7. Same as **Fig. 6**, but for the contributions and relative contributions of 25 source regions to precipitation and tropospheric total water vapour amount over SCN.
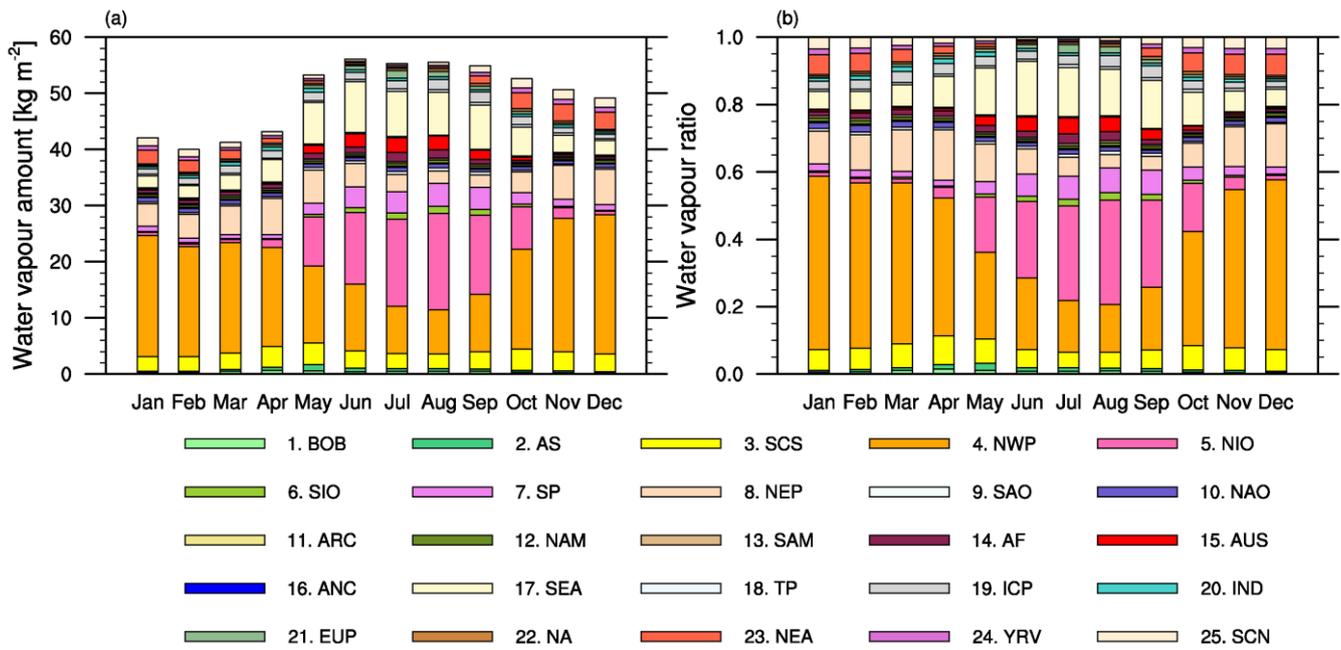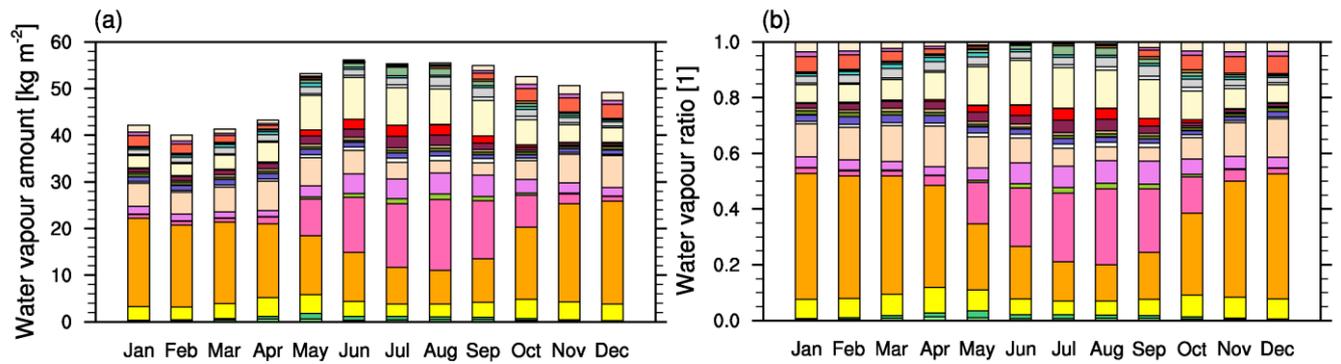
Figure 8. (a) Monthly averaged evolution of evaporative contribution of 25 defined source regions to the tropospheric total water vapour amount over the SCS. (b) Same as **Fig. 8a**, but for the relative contribution of water vapour. Stacked column colours correspond to source region colours in **Fig. 1**.